# Extended scattering-matrix method for efficient full parallel implementation of rigorous coupled-wave analysis

**Hwi Kim, Il-Min Lee, and Byoungho Lee***

*School of Electrical Engineering, Seoul National University, Kwanak-Gu Shinlim-Dong, Seoul 151-744, Korea*
**Corresponding author: byoungho@snu.ac.kr*

Received October 23, 2006; revised February 20, 2007; accepted February 26, 2007;
posted March 12, 2007 (Doc. ID 76336); published July 11, 2007

An extended and refined scattering-matrix method is proposed for the efficient full parallel implementation of rigorous coupled-wave analysis of multilayer structures. The total electromagnetic field distribution in the rigorous coupled-wave analysis is represented by the linear combination of the eigenmodes with their own coupling coefficients. In the proposed scheme, a refined recursion relation of the coupling coefficients of the eigenmodes is defined for complete parallel computation of the electromagnetic field distributions within multilayer structures. 

*OCIS codes:* 000.3860, 000.6800, 000.4430, 050.1960, 050.1950.

## 1. INTRODUCTION

Large-scale numerical analysis of Maxwell's equations is inevitable in modern nano-optics and nanophotonics. There are many branches of methodologies for numerically solving Maxwell's equations. For large-scale analyses, the exploitation of parallelism is commonly important in these methodologies. Thus novel algorithms are being actively researched to refine and improve existing methodologies to be appropriate for the parallel supercomputing environment.

The Fourier modal method (FMM) is a well-known accurate and efficient electromagnetic analysis method in the fields of nano-optics and nanophotonics. In the FMM, whole space, including target structures, is modeled by multilayer structures. The electromagnetic eigenmodes in each layer are separately characterized. In the FMM, basically, electromagnetic vector fields and structure profiles, i.e., permittivity and permeability, are represented in the Fourier domain (spatial-frequency domain or reciprocal space of the spatial domain), where the standard differential equation form of Maxwell's equations in the spatial domain is converted into an equivalent algebraic matrix eigenvalue equation of the Fourier coefficients of the electromagnetic fields. The total electromagnetic field distributions within as well as outside multilayer structures are represented by the linear combination of the eigenmodes with their own coupling coefficients. Coupling coefficients are determined to satisfy the tangential field continuation conditions on the boundaries between adjacent layers, which can be obtained by use of the scattering-matrix method (SMM) of various forms [1–4]. Additional physical information such as power flow, coupling efficiency, and separate visualization of evanescent and nonevanescent field distributions can be extracted by proper data processing of the obtained modal field information provided by the FMM. We can obtain physical intuitions on the interactions between the electromagnetic fields and structures and also exploit structural advantages of the SMM for efficient functional block-based analysis. This modal analysis is the most remarkable feature of the FMM. Within this general framework of the FMM, the possible parallelism for the practical parallel computation can be found at two points. The first parallelism lies in solving large matrix equations using the well-developed up-to-date parallel algebra libraries such as SCALAPACK. As the transversal direction supercell periods (usually $x$ and $y$-direction periods) in the FMM increase, the required number of Fourier harmonics increases rapidly. As a result, the total size of the eigenvalue equation becomes so large that the size of the FMM cannot be manageable in a single personal computer. Thus using parallel linear algebra libraries such as SCALAPACK is essential to the FMM for structures having large transversal supercell periods. This kind of parallel matrix computation has already been established in the supercomputing field.

In addition to this matrix parallelism, a different parallelism is necessary for structures having large longitudinal direction dimensions. As the longitudinal extent of a target structure becomes large, more layers are needed in the multilayer modeling of the structure. In this case, the possible parallelism can be found in the computational structure of the SMM. The SMM has its own parallelism in the associative relation that exists in the Redheffer star product of the scattering matrix ($S$-matrix). This associative relation of the Redheffer star product is exploited for the parallel computing of the FMM with the multilayer-based structure modeling. However, we note that the potential parallelism has not been fully exploited in the conventional scheme of the SMM in that the proper parallel algorithm for obtaining coupling coefficients has not been developed. In [4], it is pointed out that the main

 

computational limitation of the conventional SMM is in the calculation of coupling coefficients of the eigenmodes.

In this paper, the investigation of this second parallelism is our focus. A refined and extended formulation of the SMM is proposed for realizing efficient full parallel computation of the electromagnetic field distributions within multilayer structures. The Redheffer star product relation in the conventional SMM is defined as the recursive relation between the components of the $S$-matrix. In this paper, it is shown that a similar relation between the coupling coefficients of eigenmodes exists. The Redheffer star product relation is extended to the coupling coefficients of eigenmodes. The associative relation of the extended Redheffer star product is a key factor for the parallel computation of the electromagnetic field distributions within multilayer structures. This extended Redheffer star product relation is the main result of this paper. This scheme is so general that it can be widely applied to FMMs such as the rigorous coupled-wave analysis (RCWA) [5–9] and the pseudo-Fourier modal analysis method [10,11].

In this paper, the proposed SMM is described in the RCWA framework. The RCWA is the most popular and well-established methods among the FMMs. For proving the validity of the proposed SMM, the field distributions and coupling coefficients obtained by the enhanced transmittance matrix method (ETMM) [12] and the proposed SMM for an exemplary structure are compared. The ETMM is a well-known accurate and stable boundary-matching method, which is a serial algorithm that cannot be parallelized. It is shown that the numerical result of the SMM does highly agree with that of the ETMM.

This paper is organized as follows. In Section 2, the proposed SMM is described in the RCWA framework. The Redheffer star product relation of the coupling coefficients for the parallel computation of electromagnetic field distributions within multilayer structures is addressed. In Section 3, the advantages of the proposed SMM over the conventional SMM are discussed. In particular, the functional block-based FMM is presented as the most remarkable advantage of the proposed SMM. In Section 4, numerical results for verifying the proposed method are presented. In Section 5, the conclusion and final remarks are given.

## 2. EXTENDED SCATTERING-MATRIX METHOD

In this section, the extended SMM having the additional Redheffer star product relation of coupling coefficients of eigenmodes is described in the RCWA framework [5–7]. The main objective of the proposed SMM is the efficient parallel computation of the electromagnetic field distributions within multilayer structures.

Figure 1 shows a general multilayer structure with $N+2$ layers and $N+1$ boundaries between adjacent layers. In the RCWA, the staircase approximation is adopted in the multilayer modeling, under which each layer has permittivity and permeability profiles, being periodic in the transverse $x$ and $y$ directions, but is homogeneous along the longitudinal $z$ direction normal to the boundaries. The $n$th layer and $n$th boundary are denoted by $L_n$ and $B_n$. The total structure is composed of the input region, the multilayer body, and the output region. The multilayer body is denoted by $M^{(1,N)}$, where the superscript $(1,N)$ indicates the first and last indices of layers composing the multilayer body. The input and output regions surrounding the multilayer body are denoted by $L_0$ and $L_{N+1}$, respectively, which are half-infinite structures that may be a homogeneous space such as free space or an inhomogeneous space such as general waveguide structures.

In this paper, we conceptually distinguish two types of $S$-matrix form for convenience. One is the $S$-matrix for the characterization of the layer. The other is the $S$-matrix for the characterization of the boundary. The detailed meanings of these terms will be given in the following paragraphs.

At first, the layer $S$-matrix is considered. We adopt the mathematical induction for addressing general and complete formalism. Before the formulation of the SMM is unfolded, an understanding of the bidirectional characterization of a partial multilayer in the RCWA framework is necessary. In Fig. 2, the bidirectional characterization of a partial multilayer $M^{(n,n+m)}$ composed of consecutive $m$ layers, $L_n$–$L_{n+m}$, is illustrated, where the superscript $(n,n+m)$ indicates the first and last indices of layers composing the partial multilayer $M^{(n,n+m)}$. We assume that the partial multilayer $M^{(n,n+m)}$ is surrounded by a homogeneous and isotropic medium, i.e., free space, and the thickness of the homogeneous medium is set to zero for the domain decomposition [4]. The bidirectional characterization of the partial multilayer $M^{(n,n+m)}$ is referred to in obtaining the reflected, transmitted, and internal field distributions excited by two independent incident fields propagating in the left-to-right direction and the right-to-left direction, which are illustrated in Figs. 2(a) and 2(b), respectively. In Fig. 2, the fields propagating along the left-to-right direction and the right-to-left direction are symbolized by the superscript arrow symbols $\rightarrow$ and $\leftarrow$, respectively. The meanings of the other conventions and symbols seen in Fig. 2 are explained in the following paragraphs.

Let us first consider the left-to-right directional characterization of the partial multilayer $M^{(n,n+m)}$. In the RCWA, a set of the discrete wave vector $(k_{x,st},k_{y,st},k_{z,st})$

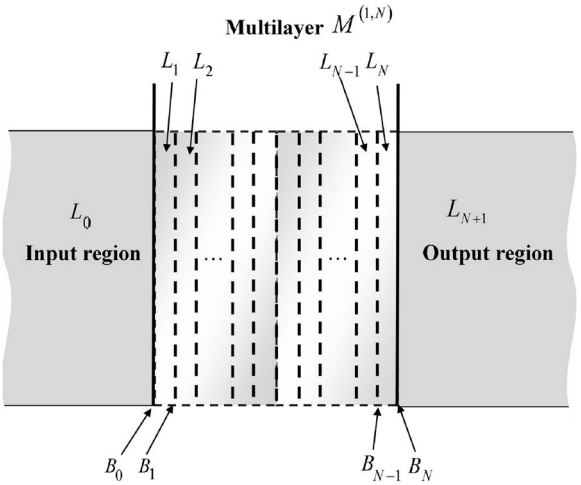


Fig. 1. Multilayer structure for the RCWA.

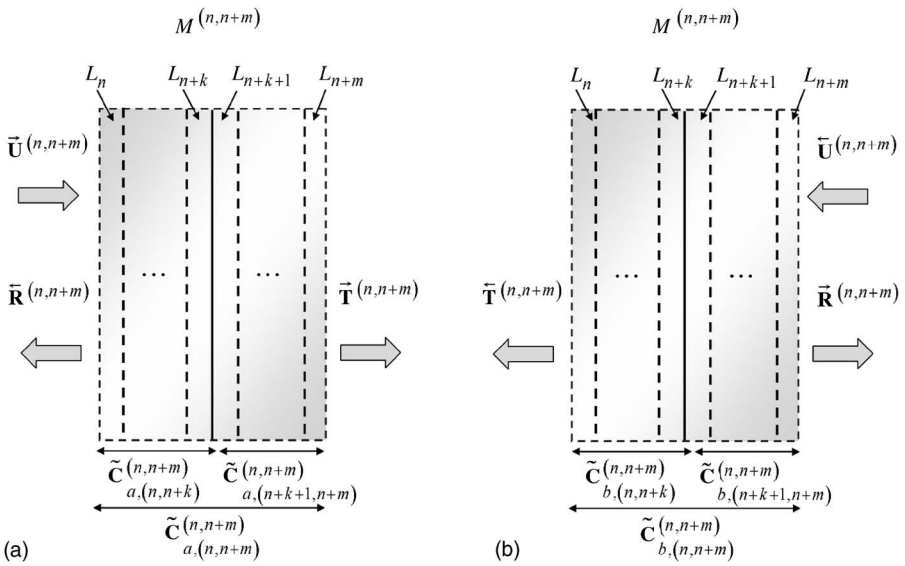


Fig. 2. Bidirectional characterization of a multilayer for obtaining the layer $S$-matrices: (a) left-to-right directional characterization, (b) right-to-left directional characterization.

indicating the $(s,t)$th diffraction channel (diffraction order) is prepared, each component of which is defined, respectively, by

$$k_{x,st} = k_x + \frac{2\pi s}{\Lambda_x}, \tag{1a}$$

$$k_{y,st} = k_y + \frac{2\pi t}{\Lambda_y}, \tag{1b}$$

$$k_{z,st} = \left(\left(\frac{2\pi}{\lambda}\right)^2 - (k_{x,st})^2 - (k_{y,st})^2\right)^{1/2}, \tag{1c}$$

where $\lambda$, $\Lambda_x$, and $\Lambda_y$ denote wavelength, the $x$-direction supercell period, and the $y$-direction supercell period, respectively. $k_x$ and $k_y$ are the $x$-direction wave-vector component and the $y$-direction wave-vector component of the 0th diffraction channel. The diffraction order indices, $s$ and $t$, are integers in the range of $-P \leq s \leq P$ and $-Q \leq t \leq Q$, respectively. In this case, the total number of Fourier harmonics used in the RCWA is $(2P+1)(2Q+1)$.

Let us assume that an input plane wave given by

$$\vec{U}_{st} = (\underline{x}\vec{u}_{x,st} + \underline{y}\vec{u}_{y,st} + \underline{z}\vec{u}_{z,st})\exp[j(k_{x,st}x + k_{y,st}y + k_{z,st}z)] \tag{2a}$$

is incident on the left boundary $B_{n-1}$ of the $n$th layer $L_n$. The plane wave of Eq. (2a) can be split into two independent polarizations, $\vec{U}_{st,(x)}$ and $\vec{U}_{st,(y)}$, respectively,

$$\vec{U}_{st,(x)} = \left(\underline{x}\vec{u}_{x,st} + \left(\frac{-\vec{u}_{x,st}k_{x,st}}{k_{z,st}}\right)\underline{z}\right) \times \exp[j(k_{x,st}x + k_{y,st}y + k_{z,st}z)], \tag{2b}$$

$$\vec{U}_{st,(y)} = \left(\underline{y}\vec{u}_{y,st} + \left(\frac{-\vec{u}_{y,st}k_{y,st}}{k_{z,st}}\right)\underline{z}\right) \times \exp[j(k_{x,st}x + k_{y,st}y + k_{z,st}z)]. \tag{2c}$$

We can see that there are two independent diffraction channels with the same wave vector. For the $(s,t)$th incident direction,$(k_{x,st},k_{y,st},k_{z,st})$, two independently polarized input excitations of Eqs. (2b) and (2c) can produce the respective reflection and transmission fields. Therefore, in the RCWA, the total number of the diffraction channels (diffraction orders) is considered to be $2(2P+1) \times (2Q+1)$, which is the twice the number of the retained Fourier harmonics.

For convenience, using the one-dimensional raw-leading ordering, let the index pair $(s,t)$ be equivalently indicated by a single index $f$ given in the range of $1 \leq f \leq 2H$, where $H$ is set to $H=(2P+1)(2Q+1)$. The relationship between the index pair $(s,t)$ and the index $f$ is defined by

$$f = (s+P)(2Q+1) + t + Q + 1 \qquad \text{for } 1 \leq f \leq H, \tag{3a}$$

$$f = (s+P)(2Q+1) + t + Q + H + 1 \qquad \text{for } H+1 \leq f \leq 2H, \tag{3b}$$

through which we can extract the index pair $(s,t)$ from the index $f$, using the above relationship. In addition, let the index $f$ in the range of $1 \leq f \leq H$ and the index $f$ in the range of $H+1 \leq f \leq 2H$ be allocated to indicate $\vec{U}_{st,(x)}$ and $\vec{U}_{st,(y)}$, respectively. In other words, we take the relations

$$\vec{U}_f = \left(\underline{y}\vec{u}_{y,st} + \left(\frac{-\vec{u}_{y,st}k_{y,st}}{k_{z,st}}\right)\underline{z}\right) \times \exp[j(k_{x,st}x + k_{y,st}y + k_{z,st}z)] \quad \text{for } 1 \leq f \leq H, \tag{4a}$$

$$\vec{U}_f = \left( \underline{x}\vec{u}_{x,st} + \left( \frac{-\vec{u}_{x,st}k_{x,st}}{k_{z,st}} \right) \underline{z} \right) \times \exp[j(k_{x,st}x + k_{y,st}y + k_{z,st}z)] \quad \text{for } H+1 \leq f \leq 2H. \tag{4b}$$

Following the above indexing scheme, the electric field distribution in the left homogeneous medium excited by the single excitation of the $f$th diffraction channel, $\underline{E}_{L,f}$, is represented by the superposition of the incident field, $\vec{U}_f$, and the reflected field as

$$\underline{E}_{L,f} = \vec{U}_f + \sum_h (\underline{x}\vec{r}_{x,hf}^{(n,n+m)} + \underline{y}\vec{r}_{y,hf}^{(n,n+m)} + \underline{z}\vec{r}_{z,hf}^{(n,n+m)}) \times \exp[j(k_{x,h}x + k_{y,h}y - k_{z,h}z)]. \tag{5a}$$

In the right homogeneous region, the transmitted electric field $\underline{E}_{R,f}$ is represented by

$$\underline{E}_{R,f} = \sum_h (\underline{x}\vec{t}_{x,hf}^{(n,n+m)} + \underline{y}\vec{t}_{y,hf}^{(n,n+m)} + \underline{z}\vec{t}_{z,hf}^{(n,n+m)}) \times \exp[j(k_{x,h}x + k_{y,h}y + k_{z,h}(z - l_{n,n+m}))], \tag{5b}$$

where the superscript $(n,n+m)$ indicates the partial multilayer $M^{(n,n+m)}$, and $(\vec{r}_{x,hf}^{(n,n+m)}, \vec{r}_{y,hf}^{(n,n+m)}, \vec{r}_{z,hf}^{(n,n+m)})$ and $(\vec{t}_{x,hf}^{(n,n+m)}, \vec{t}_{y,hf}^{(n,n+m)}, \vec{t}_{z,hf}^{(n,n+m)})$ denote the reflection coefficients and the transmission coefficients, respectively, of the $h$th diffraction channel excited by an input excitation on the $f$th diffraction channel. $l_{n,n+m}$ is the thickness of the partial multilayer $M^{(n,n+m)}$ given by $l_{n,n+m} = d_n + d_{n+1} + \cdots d_{n+m}$, where $d_k$ is the thickness of the $k$th layer.

On the other hand, let the electric and magnetic field representations in the $(n+k)$th layer $L_{n+k}$ of the partial multilayer $M^{(n,n+m)}$ be denoted by $\underline{E}_{(n+k),f}^{(n,n+m)}$ and $\underline{H}_{(n+k),f}^{(n,n+m)}$, respectively, where the subscript $f$ indicates the diffraction channel of the excitation source. In the RCWA, $\underline{E}_{(n+k),f}^{(n,n+m)}$ and $\underline{H}_{(n+k),f}^{(n,n+m)}$ take, respectively, the forms of

$$\underline{E}_{(n+k),f}^{(n,n+m)} = \sum_{p=-P}^{P} \sum_{q=-Q}^{Q} [\underline{x}S_{(n+k),x,pqf}^{(n,n+m)}(z) + \underline{y}S_{(n+k),y,pqf}^{(n,n+m)}(z) + \underline{z}S_{(n+k),z,pqf}^{(n,n+m)}(z)]\exp[j(k_{x,pq}x + k_{y,pq}y)], \tag{6a}$$

$$\underline{H}_{(n+k),f}^{(n,n+m)} = j\sqrt{\frac{\varepsilon_0}{\mu_0}} \sum_{p=-P}^{P} \sum_{q=-Q}^{Q} [\underline{x}U_{(n+k),x,pqf}^{(n,n+m)}(z) + \underline{y}U_{(n+k),y,pqf}^{(n,n+m)} \times (z) + \underline{z}U_{(n+k),z,pqf}^{(n,n+m)}(z)]\exp[j(k_{x,pq}x + k_{y,pq}y)]. \tag{6b}$$

For simplicity, following the one-dimensional raw-leading ordering defined in Eqs. (3a) and (3b), Eqs. (6a) and (6b) read, respectively, as

$$\underline{E}_{(n+k),f}^{(n,n+m)} = \sum_{h=1}^{H} [\underline{x}S_{(n+k),x,hf}^{(n,n+m)}(z) + \underline{y}S_{(n+k),y,hf}^{(n,n+m)}(z) + \underline{z}S_{(n+k),z,hf}^{(n,n+m)}(z)] \times \exp[j(k_{x,h}x + k_{y,h}y)], \tag{7a}$$

$$\underline{H}_{(n+k),f}^{(n,n+m)} = j\sqrt{\frac{\varepsilon_0}{\mu_0}} \sum_{h=1}^{H} [\underline{x}U_{(n+k),x,hf}^{(n,n+m)}(z) + \underline{y}U_{(n+k),y,hf}^{(n,n+m)}(z) + \underline{z}U_{(n+k),z,hf}^{(n,n+m)}(z)]\exp[j(k_{x,h}x + k_{y,h}y)], \tag{7b}$$

where the index pair $(p,q)$ can be equivalently indicated by the single index $h$ given by

$$h = (p+P)(2Q+1) + q + Q + 1 \quad \text{for } 1 \leq h \leq H = (2P+1)(2Q+1) \tag{7c}$$

and vector components $S_{(n+k),h}^{(n,n+m)}(z)$ and $U_{(n+k),h}^{(n,n+m)}(z)$ of the electric and magnetic fields are given, respectively, by

$$S_{(n+k),hf}^{(n,n+m)}(z) = \sum_g W_{h,g}^{(n+k)} \{c_{(n+k),gf}^{(n,n+m)+} \exp[q_g^{(n+k)}(z - l_{1,n+k-1})] + c_{(n+k),gf}^{(n,n+m)-} \exp[-q_g^{(n+k)}(z - l_{1,n+k})]\}, \tag{7d}$$

$$U_{(n+k),hf}^{(n,n+m)}(z) = \sum_g V_{h,g}^{(n+k)} \{c_{(n+k),gf}^{(n,n+m)+} \exp[q_g^{(n+k)}(z - l_{1,n+k-1})] - c_{(n+k),gf}^{(n,n+m)-} \exp[-q_g^{(n+k)}(z - l_{1,n+k})]\}, \tag{7e}$$

where notation convention follows that of [4,5]. $q_g^{(n+k)}$, $W_{h,g}^{(n+k)}$, and $V_{h,g}^{(n+k)}$ are the $g$th eigenvalue and the $g$th eigenvectors of the electric field and the magnetic field, respectively, and $l_{1,n+k}$ is given by $l_{1,n+k} = d_1 + d_2 + \cdots d_{n+k}$. It is noted in Eqs. (7d) and (7e) that the positive coupling coefficient and the negative coupling coefficient in the $(n+k)$th layer $L_{n+k}$ are distinguished and denoted by $c_{(n+k),gf}^{(n,n+m)+}$ and $c_{(n+k),gf}^{(n,n+m)-}$, respectively.

Let the column vectors of the reflection and transmission coefficients, $\vec{\mathbf{r}}_f^{(n,n+m)}$ and $\vec{\mathbf{t}}_f^{(n,n+m)}$, obtained with a specific input excitation on the $f$th diffraction channel be defined by

$$\vec{\mathbf{r}}_f^{(n,n+m)} = \begin{pmatrix} [\vec{r}_{y,hf}^{(n,n+m)}] \\ [\vec{r}_{x,hf}^{(n,n+m)}] \end{pmatrix}, \tag{8a}$$

$$\vec{\mathbf{t}}_f^{(n,n+m)} = \begin{pmatrix} [\vec{t}_{y,hf}^{(n,n+m)}] \\ [\vec{t}_{x,hf}^{(n,n+m)}] \end{pmatrix}, \tag{8b}$$

where the square brackets of $\vec{r}_{y,hf}^{(n,n+m)}$, $[\vec{r}_{y,hf}^{(n,n+m)}]$, denote a column vector with the dimensions of $H \times 1$,

$$[\vec{r}_{y,hf}^{(n,n+m)}] = (\vec{r}_{y,1f}^{(n,n+m)}, \vec{r}_{y,2f}^{(n,n+m)}, \ldots, \vec{r}_{y,Hf}^{(n,n+m)})^t. \tag{8c}$$

Thus, the dimensions of $\vec{\mathbf{r}}_f^{(n,n+m)}$ and $\vec{\mathbf{t}}_f^{(n,n+m)}$ are $2H \times 1$. Collecting all $\vec{\mathbf{r}}_f^{(n,n+m)}$ and $\vec{\mathbf{t}}_f^{(n,n+m)}$ for $f = 1,2,\cdots,2H$, we can define a reflection coefficient matrix operator $\vec{\mathbf{R}}^{(n,n+m)}$ and a transmission coefficient matrix operator $\vec{\mathbf{T}}^{(n,n+m)}$ with the dimensions of $(2H) \times (2H)$ as, respectively,

$$\vec{\mathbf{R}}^{(n,n+m)} = (\vec{\mathbf{r}}_1^{(n,n+m)}, \vec{\mathbf{r}}_2^{(n,n+m)}, \ldots, \vec{\mathbf{r}}_{2H}^{(n,n+m)}), \tag{9a}$$

$$\vec{\mathbf{T}}^{(n,n+m)} = (\vec{\mathbf{t}}_1^{(n,n+m)}, \vec{\mathbf{t}}_2^{(n,n+m)}, \ldots, \vec{\mathbf{t}}_{2H}^{(n,n+m)}). \tag{9b}$$

Then, by applying the reflection coefficient matrix operator and transmission coefficient matrix operator to the input vector $\vec{\mathbf{u}}_f$ containing the only single excitation on the $f$th diffraction channel, we can obtain the reflection and

transmission coefficient column vectors by the following operations:

$$\vec{\mathbf{r}}_f^{(n,n+m)} = \vec{\mathbf{R}}^{(n,n+m)}\vec{\mathbf{u}}_f, \tag{10a}$$

$$\vec{\mathbf{t}}_f^{(n,n+m)} = \vec{\mathbf{T}}^{(n,n+m)}\vec{\mathbf{u}}_f, \tag{10b}$$

where $\vec{\mathbf{u}}_f$ is defined by $([u_{y,f}\delta_{mf}], [u_{x,f}\delta_{mf}])^t$. Here $\delta_{mf}$ is the Kronecker delta function. Now, we take the normalized input vector, $\vec{\mathbf{u}}_f=[\delta_{mf}]$, by setting $u_{y,f}=1$ and $u_{x,f}=1$. Also, $(2H)\times(2H)$ matrix operators of the coupling coefficients, $\mathbf{C}_{a,(n+k)}^{(n,n+m)+}$ and $\mathbf{C}_{a,(n+k)}^{(n,n+m)-}$, are defined as

$$\mathbf{C}_{a,(n+k)}^{(n,n+m)+} = (\mathbf{c}_{a,(n+k),1}^{(n,n+m)+}, \mathbf{c}_{a,(n+k),2}^{(n,n+m)+}, \ldots, \mathbf{c}_{a,(n+k),2H}^{(n,n+m)+}), \tag{11a}$$

$$\mathbf{C}_{a,(n+k)}^{(n,n+m)-} = (\mathbf{c}_{a,(n+k),1}^{(n,n+m)-}, \mathbf{c}_{a,(n+k),2}^{(n,n+m)-}, \ldots, \mathbf{c}_{a,(n+k),H}^{(n,n+m)-}), \tag{11b}$$

where $\mathbf{c}_{a,(n+k),f}^{(n,n+m)+}$ and $\mathbf{c}_{a,(n+k),f}^{(n,n+m)-}$ are the column vectors of the positive coupling coefficient $c_{(n+k),gf}^{(n,n+m)+}$ and the negative coupling coefficient $c_{(n+k),gf}^{(n,n+m)-}$, respectively, defined by

$$\mathbf{c}_{a,(n+k),f}^{(n,n+m)+} = [c_{(n+k),gf}^{(n,n+m)+}], \tag{11c}$$

$$\mathbf{c}_{a,(n+k),f}^{(n,n+m)-} = [c_{(n+k),gf}^{(n,n+m)-}], \tag{11d}$$

and the subscript $a$ indicates the left-to-right directional characterization. In a similar manner in Eqs. (10a) and (10b), the coupling coefficients induced by a single input excitation on the $f$th diffraction channel are obtained as

$$\mathbf{c}_{a,(n+k),f}^{(n,n+m)+} = \mathbf{C}_{a,(n+k)}^{(n,n+m)+}\vec{\mathbf{u}}_f, \tag{11e}$$

$$\mathbf{c}_{a,(n+k),f}^{(n,n+m)-} = \mathbf{C}_{a,(n+k)}^{(n,n+m)-}\vec{\mathbf{u}}_f. \tag{11f}$$

Next, let the $(4H)\times(2H)$ coupling coefficient matrix $\mathbf{C}_{a,(n+k)}^{(n,n+m)}$ composed of the coupling coefficient matrix operators $\mathbf{C}_{a,(n+k)}^{(n,n+m)+}$ and $\mathbf{C}_{a,(n+k)}^{(n,n+m)-}$ be defined as

$$\mathbf{C}_{a,(n+k)}^{(n,n+m)} = \begin{pmatrix} \mathbf{C}_{a,(n+k)}^{(n,n+m)+} \\ \mathbf{C}_{a,(n+k)}^{(n,n+m)-} \end{pmatrix}. \tag{12a}$$

Let the set of the coupling coefficient matrix, $\mathbf{C}_{a,(n+k)}^{(n,n+m)}$, $\tilde{\mathbf{C}}_{a,(n,n+m)}^{(n,n+m)}$, be defined by

$$\tilde{\mathbf{C}}_{a,(n,n+m)}^{(n,n+m)} = \{\mathbf{C}_{a,(n)}^{(n,n+m)}, \mathbf{C}_{a,(n+1)}^{(n,n+m)}, \ldots, \mathbf{C}_{a,(n+m)}^{(n,n+m)}\}. \tag{12b}$$

In addition, let the matrix operator $\vec{\mathbf{U}}$ be defined, simply, by the $(2H)\times(2H)$ identity matrix

$$\vec{\mathbf{U}} = [\vec{\mathbf{u}}_1\ \vec{\mathbf{u}}_2\ \ldots\ \vec{\mathbf{u}}_{2H}] = \begin{bmatrix} \mathbf{I} & \mathbf{0} \\ \mathbf{0} & \mathbf{I} \end{bmatrix}, \tag{13}$$

which can be thought as the input operator expressing all possible input excitations. The matrix operators, $\vec{\mathbf{R}}^{(n,n+m)}$, $\vec{\mathbf{T}}^{(n,n+m)}$, $\mathbf{C}_{a,(n+k)}^{(n,n+m)+}$, and $\mathbf{C}_{a,(n+k)}^{(n,n+m)-}$, provide the complete information on the left-to-right directional characteristics of the partial multilayer $M^{(n,n+m)}$.

On the other hand, let us consider the right-to-left directional characterization of the partial multilayer $M^{(n,n+m)}$. In this case, the input field in the right homogeneous region is represented by

$$\tilde{U}_f = (\underline{x}\tilde{u}_{x,f} + \underline{y}\tilde{u}_{y,f} + \underline{z}\tilde{u}_{z,f})\exp[j(k_{x,f}x + k_{y,f}y - k_{z,f}(z - d_{n,n+m}))]. \tag{14a}$$

In the right homogeneous region, the electric field distribution $\underline{E}_{R,f}$ is represented by the superposition of the incident field and the reflected field distributions as

$$\underline{E}_{R,f} = \tilde{U}_f + \sum_h (\underline{x}\vec{r}_{x,hf}^{(n,n+m)} + \underline{y}\vec{r}_{y,hf}^{(n,n+m)} + \underline{z}\vec{r}_{z,hf}^{(n,n+m)}) \times \exp[j(k_{x,h}x + k_{y,h}y + k_{z,h}(z - d_{n,n+m}))]. \tag{14b}$$

In the left homogeneous region, the transmitted electric field is represented by

$$\tilde{E}_{L,f} = \sum_h (\underline{x}\tilde{t}_{x,hf}^{(n,n+m)} + \underline{y}\tilde{t}_{y,hf}^{(n,n+m)} + \underline{z}\tilde{t}_{z,hf}^{(n,n+m)}) \times \exp[j(k_{x,h}x + k_{y,h}y - k_{z,h}z)]. \tag{14c}$$

In the same way as in the case of the left-to-right directional characterization, we can define the matrix operators $\tilde{\mathbf{U}}^{(n,n+m)}$, $\vec{\mathbf{R}}^{(n,n+m)}$, $\vec{\mathbf{T}}^{(n,n+m)}$, $\mathbf{C}_{b,(n+k)}^{(n,n+m)+}$, and $\mathbf{C}_{b,(n+k)}^{(n,n+m)-}$ in the right-to-left directional characterization of the partial multilayer $M^{(n,n+m)}$. In the definitions of $\mathbf{C}_{b,(n+k)}^{(n,n+m)+}$ and $\mathbf{C}_{b,(n+k)}^{(n,n+m)-}$, the subscript $b$ indicates the right-to-left directional characterization. In practice, for the right-to-left directional characterization, we just have to reverse the optic axis in the RCWA without making any changes in the multilayer structure. However, considering that the optic axis is reversed, we can define the $(4H)\times(2H)$ coupling coefficient matrix $\mathbf{C}_{b,(n+k)}^{(n,n+m)}$ composed of the coupling coefficient matrix operators $\mathbf{C}_{b,(n+k)}^{(n,n+m)+}$ and $\mathbf{C}_{b,(n+k)}^{(n,n+m)-}$, in contrast to the definition of $\mathbf{C}_{a,(n+k)}^{(n,n+m)}$ in Eq. (12a), as

$$\mathbf{C}_{b,(n+k)}^{(n,n+m)} = \begin{pmatrix} \mathbf{C}_{b,(n+k)}^{(n,n+m)-} \\ \mathbf{C}_{b,(n+k)}^{(n,n+m)+} \end{pmatrix}. \tag{15a}$$

Then the set of the coupling coefficient matrix $\mathbf{C}_{b,(n+k)}^{(n,n+m)}$ is defined by

$$\tilde{\mathbf{C}}_{b,(n,n+m)}^{(n,n+m)} = \{\mathbf{C}_{b,(n)}^{(n,n+m)}, \mathbf{C}_{b,(n+1)}^{(n,n+m)}, \ldots, \mathbf{C}_{b,(n+m)}^{(n,n+m)}\}. \tag{15b}$$

In the proposed SMM scheme, the above-stated operators, $\vec{\mathbf{R}}^{(n,n+m)}$, $\vec{\mathbf{T}}^{(n,n+m)}$, $\tilde{\mathbf{R}}^{(n,n+m)}$, and $\tilde{\mathbf{T}}^{(n,n+m)}$, compose the layer $S$-matrix $\mathbf{S}^{(n,n+m)}$ of the partial multilayer $M^{(n,n+m)}$, taking the form

$$\mathbf{S}^{(n,n+m)} = \begin{bmatrix} \vec{\mathbf{T}}^{(n,n+m)} & \tilde{\mathbf{R}}^{(n,n+m)} \\ \vec{\mathbf{R}}^{(n,n+m)} & \tilde{\mathbf{T}}^{(n,n+m)} \end{bmatrix}. \tag{16}$$

With the above-defined symbols, the relationship between the layer $S$-matrix components of the larger partial multilayer $M^{(n,n+m+l)}$ and the layer $S$-matrix components of two subpartial multilayers $M^{(n,n+m)}$ and $M^{(n+m+1,n+m+l)}$ making up $M^{(n,n+m+l)}$ can be constructed. Conventionally, this relation is called the Redheffer star product of the SMM. The Redheffer star product relation can be intuitively derived based on the physical process of infinite multiple reflections between adjacent partial multilayer blocks as indicated in Fig. 3.

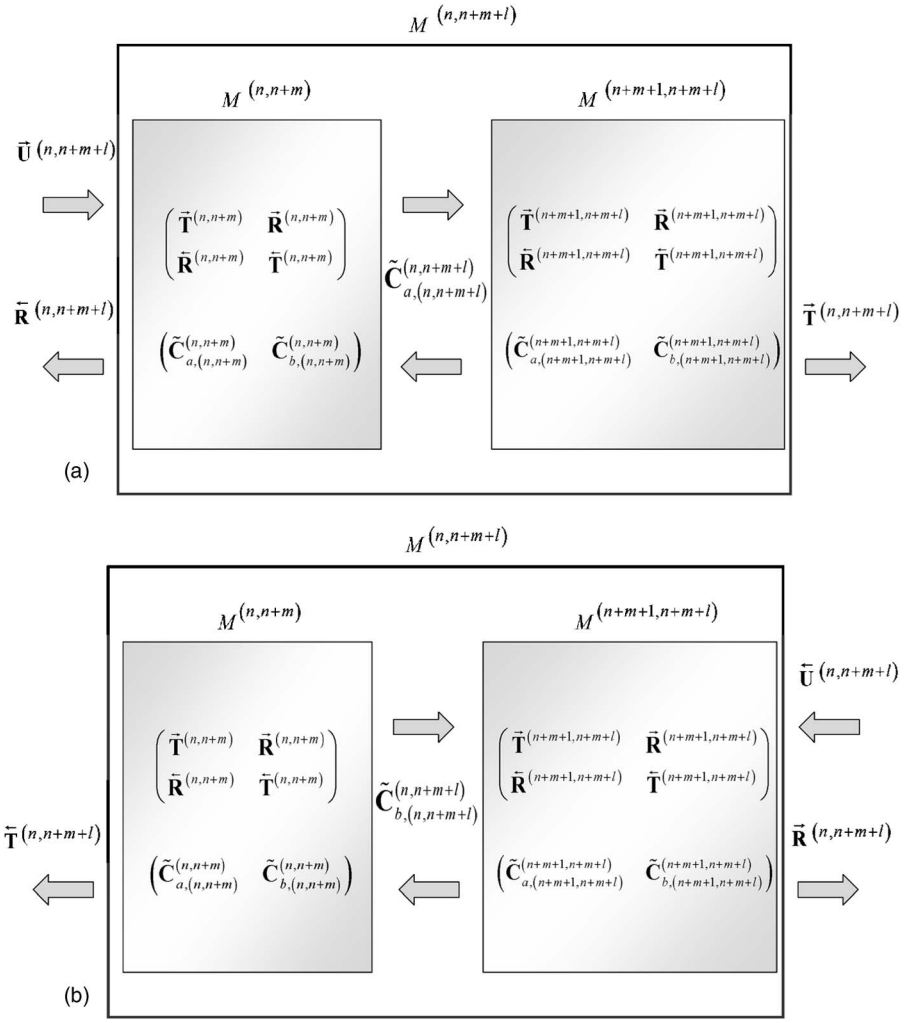


Fig. 3. Intuitive derivation of the Redheffer star product relation through (a) the left-to-right directional characterization, (b) the right-to-left directional characterization of the combined multilayer.

In the proposed SMM scheme, the relationship between coupling coefficient matrices of the larger partial multilayer $M^{(n,n+m+l)}$ and those of the subpartial multilayers $M^{(n,n+m)}$ and $M^{(n+m+1,n+m+l)}$ is also manifested. This relationship can be called the extended Redheffer star product of the coupling coefficients.

The infinite multiple reflections between multilayer blocks, $M^{(n,n+m)}$ and $M^{(n+m+1,n+m+l)}$, can be easily analyzed by a simple ray-tracing approach. The relationships among the layer $S$-matrix components of $M^{(n,n+m)}$, $M^{(n+m+1,n+m+l)}$, and $M^{(n,n+m+l)}$ are stated as follows:

$$\begin{aligned}\overleftarrow{\mathbf{R}}^{(n,n+m+l)} &= \overleftarrow{\mathbf{R}}^{(n,n+m)} + \overleftarrow{\mathbf{T}}^{(n,n+m)}\left[\sum_{k=0}^{\infty}(\overleftarrow{\mathbf{R}}^{(n+m+1,n+m+l)}\vec{\mathbf{R}}^{(n,n+m)})^k\right]\\ &\quad\times\overleftarrow{\mathbf{R}}^{(n+m+1,n+m+l)}\vec{\mathbf{T}}^{(n,n+m)}\\ &= \overleftarrow{\mathbf{R}}^{(n,n+m)} + \overleftarrow{\mathbf{T}}^{(n,n+m)}(\mathbf{I}-\overleftarrow{\mathbf{R}}^{(n+m+1,n+m+l)}\vec{\mathbf{R}}^{(n,n+m)})^{-1}\\ &\quad\times\overleftarrow{\mathbf{R}}^{(n+m+1,n+m+l)}\vec{\mathbf{T}}^{(n,n+m)},\end{aligned} \tag{17a}$$

$$\begin{aligned}\vec{\mathbf{T}}^{(n,n+m+l)} &= \vec{\mathbf{T}}^{(n+m+1,n+m+l)}\\ &\quad\times\left[\sum_{k=0}^{\infty}(\vec{\mathbf{R}}^{(n,n+m)}\overleftarrow{\mathbf{R}}^{(n+m+1,n+m+l)})^k\right]\vec{\mathbf{T}}^{(n,n+m)}\\ &= \vec{\mathbf{T}}^{(n+m+1,n+m+l)}(\mathbf{I}-\vec{\mathbf{R}}^{(n,n+m)}\\ &\quad\times\overleftarrow{\mathbf{R}}^{(n+m+1,n+m+l)})^{-1}\vec{\mathbf{T}}^{(n,n+m)},\end{aligned} \tag{17b}$$

$$\begin{aligned}\vec{\mathbf{R}}^{(n,n+m+l)} &= \vec{\mathbf{R}}^{(n+m+1,n+m+l)} + \vec{\mathbf{T}}^{(n+m+1,n+m+l)}\\ &\quad\times\left[\sum_{k=0}^{\infty}(\vec{\mathbf{R}}^{(n,n+m)}\overleftarrow{\mathbf{R}}^{(n+m+1,n+m+l)})^k\right]\\ &\quad\times\vec{\mathbf{R}}^{(n,n+m)}\vec{\mathbf{T}}^{(n+m+1,n+m+l)}\\ &= \vec{\mathbf{R}}^{(n+m+1,n+m+l)} + \vec{\mathbf{T}}^{(n+m+1,n+m+l)}\\ &\quad\times(\mathbf{I}-\vec{\mathbf{R}}^{(n,n+m)}\overleftarrow{\mathbf{R}}^{(n+m+1,n+m+l)})^{-1}\\ &\quad\times\vec{\mathbf{R}}^{(n,n+m)}\vec{\mathbf{T}}^{(n+m+1,n+m+l)},\end{aligned} \tag{17c}$$

$$\overleftarrow{\mathbf{T}}^{(n,n+m+l)} = \overleftarrow{\mathbf{T}}^{(n,n+m)}\left[\sum_{k=0}^{\infty}(\overleftarrow{\mathbf{R}}^{(n+m+1,n+m+l)}\overrightarrow{\mathbf{R}}^{(n,n+m)})^k\right] \times \overleftarrow{\mathbf{T}}^{(n+m+1,n+m+l)}$$
$$= \overleftarrow{\mathbf{T}}^{(n,n+m)}(\mathbf{I} - \overleftarrow{\mathbf{R}}^{(n+m+1,n+m+l)}\overrightarrow{\mathbf{R}}^{(n,n+m)})^{-1}\overleftarrow{\mathbf{T}}^{(n+m+1,n+m+l)}. \quad (17d)$$

The above-obtained relations are the well-known Redheffer star product relation of the SMM. This relationship is symbolized by the star product of the layer $S$-matrices as

$$\mathbf{S}^{(n,n+m+l)} = \mathbf{S}^{(n,n+m)} * \mathbf{S}^{(n+m+1,n+m+l)}. \quad (18)$$

The Redheffer star product can be understood as the infinite sum of multiple reflections and transmissions between adjacent multilayer blocks.

We also see that, during multiple reflections, the internal coupling coefficient matrices of all layers are updated, since the whole process is linear and the coupling coefficient is linearly proportional to the external field. Hence, the internal coupling coefficients in the combined multilayer $M^{(n,n+m+l)}$ can also be recursively extracted by a similar formula. The set of the coupling coefficient matrices $\tilde{\mathbf{C}}^{(n,n+m+l)}_{a,(n,n+m+l)}$ and $\tilde{\mathbf{C}}^{(n,n+m+l)}_{b,(n,n+m+l)}$ of the combined multilayer $M^{(n,n+m+l)}$ are divided into two subparts as, respectively,

$$\tilde{\mathbf{C}}^{(n,n+m+l)}_{a,(n,n+m+l)} = \{\tilde{\mathbf{C}}^{(n,n+m+l)}_{a,(n,n+m)}, \tilde{\mathbf{C}}^{(n,n+m+l)}_{a,(n+m+1,n+m+l)}\}, \quad (19a)$$

$$\tilde{\mathbf{C}}^{(n,n+m+l)}_{b,(n,n+m+l)} = \{\tilde{\mathbf{C}}^{(n,n+m+l)}_{b,(n,n+m)}, \tilde{\mathbf{C}}^{(n,n+m+l)}_{b,(n+m+1,n+m+l)}\}, \quad (19b)$$

where the subsets $\tilde{\mathbf{C}}^{(n,n+m+l)}_{a,(n,n+m)}$, $\tilde{\mathbf{C}}^{(n,n+m+l)}_{a,(n+m+1,n+m+l)}$, $\tilde{\mathbf{C}}^{(n,n+m+l)}_{b,(n,n+m)}$, and $\tilde{\mathbf{C}}^{(n,n+m+l)}_{b,(n+m+1,n+m+l)}$ are given, respectively, by

$$\tilde{\mathbf{C}}^{(n,n+m+l)}_{a,(n,n+m)} = \{\mathbf{C}^{(n,n+m+l)}_{a,(n)}, \mathbf{C}^{(n,n+m+l)}_{a,(n+1)}, \ldots, \mathbf{C}^{(n,n+m+l)}_{a,(n+m)}\}, \quad (19c)$$

$$\tilde{\mathbf{C}}^{(n,n+m+l)}_{a,(n+m+1,n+m+l)} = \{\mathbf{C}^{(n,n+m+l)}_{a,(n+m+1)}, \mathbf{C}^{(n,n+m+l)}_{a,(n+m+2)}, \ldots, \mathbf{C}^{(n,n+m+l)}_{a,(n+m+l)}\}, \quad (19d)$$

$$\tilde{\mathbf{C}}^{(n,n+m+l)}_{b,(n,n+m)} = \{\mathbf{C}^{(n,n+m+l)}_{b,(n)}, \mathbf{C}^{(n,n+m+l)}_{b,(n+1)}, \ldots, \mathbf{C}^{(n,n+m+l)}_{b,(n+m)}\}, \quad (19e)$$

$$\tilde{\mathbf{C}}^{(n,n+m+l)}_{b,(n+m+1,n+m+l)} = \{\mathbf{C}^{(n,n+m+l)}_{b,(n+m+1)}, \mathbf{C}^{(n,n+m+l)}_{b,(n+m+2)}, \ldots, \mathbf{C}^{(n,n+m+l)}_{b,(n+m+l)}\}. \quad (19f)$$

The respective updated pairs of the set of the coupling coefficient matrices $(\tilde{\mathbf{C}}^{(n,n+m+l)}_{a,(n,n+m)}, \tilde{\mathbf{C}}^{(n,n+m+l)}_{b,(n,n+m)})$ and $(\tilde{\mathbf{C}}^{(n,n+m+l)}_{a,(n+m+1,n+m+l)}, \tilde{\mathbf{C}}^{(n,n+m+l)}_{b,(n+m+1,n+m+l)})$ in the part of layers $L_n - L_{n+m}$ and in the part of layers $L_{n+m+1} - L_{n+m+l}$ are obtained by the following relations. For $k$ in the range of $n \leqslant k \leqslant n+m$, the $(4H)\times(2H)$ coupling coefficient matrices, $\mathbf{C}^{(n,n+m+l)}_{a,(k)}$ and $\mathbf{C}^{(n,n+m+l)}_{b,(k)}$, are derived as

$$\mathbf{C}^{(n,n+m+l)}_{a,(k)} = \mathbf{C}^{(n,n+m)}_{a,(k)} + \mathbf{C}^{(n,n+m)}_{b,(k)}(\mathbf{I} - \overleftarrow{\mathbf{R}}^{(n+m+1,n+m+l)}\overrightarrow{\mathbf{R}}^{(n,n+m)})^{-1} \times \overleftarrow{\mathbf{R}}^{(n+m+1,n+m+l)}\overrightarrow{\mathbf{T}}^{(n,n+m)}, \quad (20a)$$

$$\mathbf{C}^{(n,n+m+l)}_{b,(k)} = \mathbf{C}^{(n,n+m)}_{b,(k)}(\mathbf{I} - \overleftarrow{\mathbf{R}}^{(n+m+1,n+m+l)} \times \overrightarrow{\mathbf{R}}^{(n,n+m)})^{-1}\overleftarrow{\mathbf{T}}^{(n+m+1,n+m+l)}. \quad (20b)$$

For $k$ in the range of $n+m+1 \leqslant k \leqslant n+m+l$, the coupling coefficient matrices, $\mathbf{C}^{(n,n+m+l)}_{a,(k)}$ and $\mathbf{C}^{(n,n+m+l)}_{b,(k)}$, are derived as

$$\mathbf{C}^{(n,n+m+l)}_{a,(k)} = \mathbf{C}^{(n+m+1,n+m+l)}_{a,(k)}(\mathbf{I} - \overrightarrow{\mathbf{R}}^{(n,n+m)}\overleftarrow{\mathbf{R}}^{(n+m+1,n+m+l)})^{-1}\overrightarrow{\mathbf{T}}^{(n,n+m)}, \quad (20c)$$

$$\mathbf{C}^{(n,n+m+l)}_{b,(k)} = \mathbf{C}^{(n+m+1,n+m+l)}_{b,(k)} + \mathbf{C}^{(n+m+1,n+m+l)}_{a,(k)} \times (\mathbf{I} - \overrightarrow{\mathbf{R}}^{(n,n+m)}\overleftarrow{\mathbf{R}}^{(n+m+1,n+m+l)})^{-1} \times \overrightarrow{\mathbf{R}}^{(n,n+m)}\overleftarrow{\mathbf{T}}^{(n+m+1,n+m+l)}. \quad (20d)$$

This relationship can be symbolized, using the notations in Eqs. (19a) and (19b), as

$$(\tilde{\mathbf{C}}^{(n,n+m+l)}_{a,(n,n+m+l)}, \tilde{\mathbf{C}}^{(n,n+m+l)}_{b,(n,n+m+l)}) = (\tilde{\mathbf{C}}^{(n,n+m)}_{a,(n,n+m)}, \tilde{\mathbf{C}}^{(n,n+m)}_{b,(n,n+m)}) * (\tilde{\mathbf{C}}^{(n+m+1,n+m+l)}_{a,(n+m+1,n+m+l)}, \times \tilde{\mathbf{C}}^{(n+m+1,n+m+l)}_{b,(n+m+1,n+m+l)}). \quad (21)$$

This is the extended Redheffer star product of the coupling coefficient matrices. Considering the physical process of infinite multiple reflections and transmissions between adjacent multilayer blocks, we can see that the associative rules definitely exist in the derived Redheffer star product relation of the coupling coefficients as well as in the known Redheffer star product relation of the $S$-matrix components. These associative rules enable the parallel computation of the internal coupling coefficients.

Finally, with the aid of the associative rule, the layer $S$-matrix and the coupling coefficient matrix of the multilayer $M^{(1,N)}$ can be obtained by

$$\mathbf{S}^{(1,N)} = \mathbf{S}^{(1,1)} * \mathbf{S}^{(2,2)} * \cdots * \mathbf{S}^{(N-1,N-1)} * \mathbf{S}^{(N,N)}, \quad (22a)$$

$$(\tilde{\mathbf{C}}^{(1,N)}_{a,(1,N)}, \tilde{\mathbf{C}}^{(1,N)}_{b,(1,N)}) = (\tilde{\mathbf{C}}^{(1,1)}_{a,(1,1)}, \tilde{\mathbf{C}}^{(1,1)}_{b,(1,1)}) * (\tilde{\mathbf{C}}^{(2,2)}_{a,(2,2)}, \tilde{\mathbf{C}}^{(2,2)}_{b,(2,2)}) * \cdots * \times (\tilde{\mathbf{C}}^{(N-1,N-1)}_{a,(N-1,N-1)}, \tilde{\mathbf{C}}^{(N-1,N-1)}_{b,(N-1,N-1)}) * (\tilde{\mathbf{C}}^{(N,N)}_{a,(N,N)}, \tilde{\mathbf{C}}^{(N,N)}_{b,(N,N)}). \quad (22b)$$

For achieving the completeness of the mathematical induction, we should address the practical calculation of the layer $S$-matrices of a single layer through the bidirectional characterization with the RCWA. Considering the $n$th layer, we can find the reflection coefficient matrix operators and transmission coefficient matrix operators as follows. In the case of left-to-right directional character-

ization, the boundary conditions at both left and right boundaries are described as, respectively,

$$\begin{bmatrix} \mathbf{W}_h & \mathbf{W}_h \\ \mathbf{V}_h & -\mathbf{V}_h \end{bmatrix} \begin{pmatrix} \vec{\mathbf{U}} \\ \overleftarrow{\mathbf{R}}^{(n,n)} \end{pmatrix} = \begin{bmatrix} \mathbf{W}^{(n)} & \mathbf{W}^{(n)}\mathbf{X}^{(n)} \\ \mathbf{V}^{(n)} & -\mathbf{V}^{(n)}\mathbf{X}^{(n)} \end{bmatrix} \begin{pmatrix} \mathbf{C}_{a,(n)}^{(n,n)+} \\ \mathbf{C}_{a,(n)}^{(n,n)-} \end{pmatrix}, \tag{23a}$$

$$\begin{bmatrix} \mathbf{W}^{(n)}\mathbf{X}^{(n)} & \mathbf{W}^{(n)} \\ \mathbf{V}^{(n)}\mathbf{X}^{(n)} & -\mathbf{V}^{(n)} \end{bmatrix} \begin{pmatrix} \mathbf{C}_{a,(n)}^{(n,n)+} \\ \mathbf{C}_{a,(n)}^{(n,n)-} \end{pmatrix} = \begin{pmatrix} \mathbf{W}_h \\ \mathbf{V}_h \end{pmatrix} \vec{\mathbf{T}}^{(n,n)}. \tag{23b}$$

The following procedure is preferred for stably solving Eqs. (23a) and (23b),

$$\begin{pmatrix} \mathbf{C}_{a,(n)}^{(n,n)+} \\ \mathbf{C}_{a,(n)}^{(n,n)-} \end{pmatrix} = \begin{bmatrix} \mathbf{W}_h^{-1}\mathbf{W}^{(n)} + \mathbf{V}_h^{-1}\mathbf{V}^{(n)} & (\mathbf{W}_h^{-1}\mathbf{W}^{(n)} - \mathbf{V}_h^{-1}\mathbf{V}^{(n)})\mathbf{X}^{(n)} \\ (\mathbf{W}_h^{-1}\mathbf{W}^{(n)} - \mathbf{V}_h^{-1}\mathbf{V}^{(n)})\mathbf{X}^{(n)} & \mathbf{W}_h^{-1}\mathbf{W}^{(n)} + \mathbf{V}_h^{-1}\mathbf{V}^{(n)} \end{bmatrix}^{-1} \begin{pmatrix} 2\vec{\mathbf{U}} \\ \mathbf{0} \end{pmatrix}, \tag{24a}$$

$$\overleftarrow{\mathbf{R}}^{(n,n)} = \mathbf{W}_h^{-1}[\mathbf{W}^{(n)}\mathbf{C}_{a,(n)}^{(n,n)+} + \mathbf{W}^{(n)}\mathbf{X}^{(n)}\mathbf{C}_{a,(n)}^{(n,n)-} - \mathbf{W}_h\vec{\mathbf{U}}], \tag{24b}$$

$$\vec{\mathbf{T}}^{(n,n)} = \mathbf{W}_h^{-1}[\mathbf{W}^{(n)}\mathbf{X}^{(n)}\mathbf{C}_{a,(n)}^{(n,n)+} + \mathbf{W}^{(n)}\mathbf{C}_{a,(n)}^{(n,n)-}], \tag{24c}$$

where $\mathbf{W}^{(n)}$, $\mathbf{V}^{(n)}$, and $\mathbf{X}^{(n)}$ are the eigenvector matrices of the electric field and the magnetic field in the layer $L_n$ and the diagonal matrix of exponentials of eigenvalues, respectively. $\mathbf{W}_h$ and $\mathbf{V}_h$ are the eigenvector matrices of the electric field and magnetic field in the surrounding medium given by, respectively,

$$\mathbf{W}_h = \begin{bmatrix} \mathbf{I} & \mathbf{0} \\ \mathbf{0} & \mathbf{I} \end{bmatrix}, \tag{25a}$$

$$\mathbf{V}_h = \begin{bmatrix} \left[\dfrac{k_{x,st}k_{y,st}}{jk_0k_{I,z,st}}\right] & \left[\dfrac{(k_{I,z,st}^2 + k_{x,st}^2)}{jk_0k_{I,z,st}}\right] \\ \left[-\dfrac{(k_{y,st}^2 + k_{I,z,st}^2)}{jk_0k_{I,z,st}}\right] & \left[-\dfrac{k_{y,st}k_{x,st}}{jk_0k_{I,z,st}}\right] \end{bmatrix}. \tag{25b}$$

In the case of the right-to-left directional characterization, the boundary conditions at both left and right boundaries are described as, respectively,

$$\begin{pmatrix} \mathbf{W}_h \\ -\mathbf{V}_h \end{pmatrix} \overleftarrow{\mathbf{T}}^{(n,n)} = \begin{bmatrix} \mathbf{W}^{(n)}\mathbf{X}^{(n)} & \mathbf{W}^{(n)} \\ -\mathbf{V}^{(n)}\mathbf{X}^{(n)} & \mathbf{V}^{(n)} \end{bmatrix} \begin{pmatrix} \mathbf{C}_{b,(n)}^{(n,n)-} \\ \mathbf{C}_{b,(n)}^{(n,n)+} \end{pmatrix}, \tag{26a}$$

$$\begin{bmatrix} \mathbf{W}^{(n)} & \mathbf{W}^{(n)}\mathbf{X}^{(n)} \\ -\mathbf{V}^{(n)} & \mathbf{V}^{(n)}\mathbf{X}^{(n)} \end{bmatrix} \begin{pmatrix} \mathbf{C}_{b,(n)}^{(n,n)-} \\ \mathbf{C}_{b,(n)}^{(n,n)+} \end{pmatrix} = \begin{bmatrix} \mathbf{W}_h & \mathbf{W}_h \\ -\mathbf{V}_h & \mathbf{V}_h \end{bmatrix} \begin{pmatrix} \overleftarrow{\mathbf{U}} \\ \vec{\mathbf{R}}^{(n,n)} \end{pmatrix}. \tag{26b}$$

The following procedure is taken for stably solving Eqs. (26a) and (26b):

$$\begin{pmatrix} \mathbf{C}_{b,(n)}^{(n,n)-} \\ \mathbf{C}_{b,(n)}^{(n,n)+} \end{pmatrix} = \begin{bmatrix} \mathbf{W}_h^{-1}\mathbf{W}^{(n)} + \mathbf{V}_h^{-1}\mathbf{V}^{(n)} & (\mathbf{W}_h^{-1}\mathbf{W}^{(n)} - \mathbf{V}_h^{-1}\mathbf{V}^{(n)})\mathbf{X}^{(n)} \\ (\mathbf{W}_h^{-1}\mathbf{W}^{(n)} - \mathbf{V}_h^{-1}\mathbf{V}^{(n)})\mathbf{X}^{(n)} & \mathbf{W}_h^{-1}\mathbf{W}^{(n)} + \mathbf{V}_h^{-1}\mathbf{V}^{(n)} \end{bmatrix}^{-1} \times \begin{pmatrix} 2\overleftarrow{\mathbf{U}} \\ \mathbf{0} \end{pmatrix}, \tag{27a}$$

$$\vec{\mathbf{R}}^{(n,n)} = \mathbf{W}_h^{-1}[\mathbf{W}^{(n)}\mathbf{C}_{b,(n)}^{(n,n)-} + \mathbf{W}^{(n)}\mathbf{X}^{(n)}\mathbf{C}_{b,(n)}^{(n,n)+} - \mathbf{W}_h\vec{\mathbf{U}}], \tag{27b}$$

$$\overleftarrow{\mathbf{T}}^{(n,n)} = \mathbf{W}_h^{-1}[\mathbf{W}^{(n)}\mathbf{X}^{(n)}\mathbf{C}_{b,(n)}^{(n,n)-} + \mathbf{W}^{(n)}\mathbf{C}_{b,(n)}^{(n,n)+}]. \tag{27c}$$

Comparing Eqs. (24a)–(24c) and Eqs. (27a)–(27c), we can see that the following equalities actually hold:

$$\overleftarrow{\mathbf{R}}^{(n,n)} = \vec{\mathbf{R}}^{(n,n)}, \tag{28a}$$

$$\vec{\mathbf{T}}^{(n,n)} = \overleftarrow{\mathbf{T}}^{(n,n)}, \tag{28b}$$

$$\begin{pmatrix} \mathbf{C}_{a,(n)}^{(n,n)+} \\ \mathbf{C}_{a,(n)}^{(n,n)-} \end{pmatrix} = \begin{pmatrix} \mathbf{C}_{b,(n)}^{(n,n)-} \\ \mathbf{C}_{b,(n)}^{(n,n)+} \end{pmatrix}. \tag{28c}$$

These equalities are due to the staircase approximation adopted in the RCWA and used in the practical computation.

Next, the boundary $S$-matrices for the boundaries $B_0$ and $B_N$ are derived. The bidirectional characterization of the boundaries $B_0$ and $B_N$ for obtaining the boundary $S$-matrices is illustrated in Figs. 4(a) and 4(b), respectively. As mentioned previously, the input and the output layers, $L_0$ and $L_{N+1}$, are actually half-infinite layers. Hence the boundary $S$-matrices must be manifested to connect these half-infinite layers to the finite body of the multilayer $M^{(1,N)}$:

$$\mathbf{S}^{(0,0)} = \begin{bmatrix} \vec{\mathbf{T}}^{(0,0)} & \vec{\mathbf{R}}^{(0,0)} \\ \overleftarrow{\mathbf{R}}^{(0,0)} & \overleftarrow{\mathbf{T}}^{(0,0)} \end{bmatrix}, \tag{29a}$$

where $\vec{\mathbf{T}}^{(0,0)}$, $\overleftarrow{\mathbf{R}}^{(0,0)}$, $\overleftarrow{\mathbf{T}}^{(0,0)}$, and $\vec{\mathbf{R}}^{(0,0)}$ are given by, respectively,

$$\vec{\mathbf{T}}^{(0,0)} = 2[(\mathbf{W}^{(0)})^{-1}\mathbf{W}_h + (\mathbf{V}^{(0)})^{-1}\mathbf{V}_h]^{-1}, \tag{29b}$$

$$\overleftarrow{\mathbf{R}}^{(0,0)} = [(\mathbf{W}_h)^{-1}\mathbf{W}^{(0)} + (\mathbf{V}_h)^{-1}\mathbf{V}^{(0)}]^{-1} \times [-(\mathbf{W}_h)^{-1}\mathbf{W}^{(0)} + (\mathbf{V}_h)^{-1}\mathbf{V}^{(0)}], \tag{29c}$$

$$\overleftarrow{\mathbf{T}}^{(0,0)} = 2[(\mathbf{W}_h)^{-1}\mathbf{W}^{(0)} + (\mathbf{V}_h)^{-1}\mathbf{V}^{(0)}]^{-1}, \tag{29d}$$

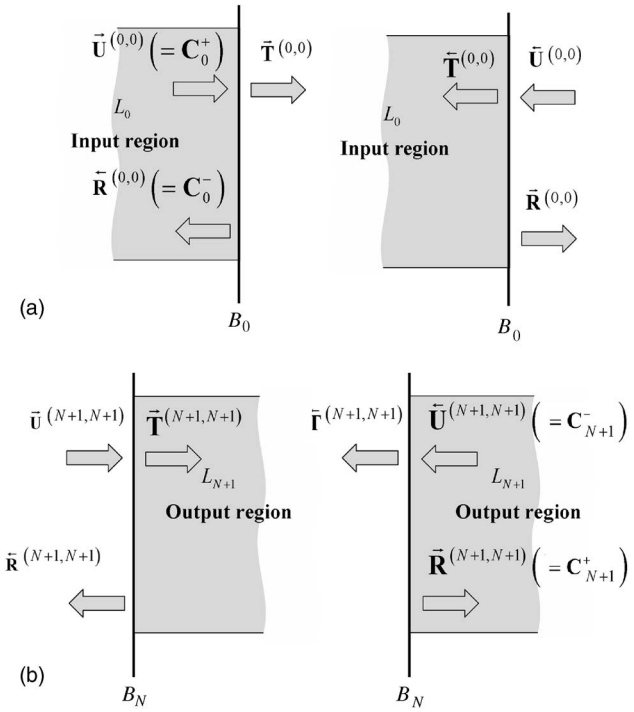


Fig. 4. Bidirectional characterization of (a) the boundary $B_0$ and (b) the boundary $B_N$.

$$\vec{\mathbf{R}}^{(0,0)} = [(\mathbf{W}^{(0)})^{-1}\mathbf{W}_h + (\mathbf{V}^{(0)})^{-1}\mathbf{V}_h]^{-1} \times [-(\mathbf{W}^{(0)})^{-1}\mathbf{W}_h + (\mathbf{V}^{(0)})^{-1}\mathbf{V}_h]. \quad (29e)$$

The boundary $S$-matrix of the boundary $B_N$ is also obtained as

$$\mathbf{S}^{(N+1,N+1)} = \begin{bmatrix} \vec{\mathbf{T}}^{(N+1,N+1)} & \vec{\mathbf{R}}^{(N+1,N+1)} \\ \overleftarrow{\mathbf{R}}^{(N+1,N+1)} & \overleftarrow{\mathbf{T}}^{(N+1,N+1)} \end{bmatrix}, \quad (30a)$$

where $\vec{\mathbf{T}}^{(N+1,N+1)}$, $\overleftarrow{\mathbf{R}}^{(N+1,N+1)}$, $\overleftarrow{\mathbf{T}}^{(N+1,N+1)}$, and $\vec{\mathbf{R}}^{(N+1,N+1)}$ are given by, respectively,

$$\vec{\mathbf{T}}^{(N+1,N+1)} = 2[(\mathbf{W}_h)^{-1}\mathbf{W}^{(N+1)} + (\mathbf{V}_h)^{-1}\mathbf{V}^{(N+1)}]^{-1}, \quad (30b)$$

$$\overleftarrow{\mathbf{R}}^{(N+1,N+1)} = [(\mathbf{W}^{(N+1)})^{-1}\mathbf{W}_h + (\mathbf{V}^{(N+1)})^{-1}\mathbf{V}_h]^{-1} \times [-(\mathbf{W}^{(N+1)})^{-1}\mathbf{W}_h + (\mathbf{V}^{(N+1)})^{-1}\mathbf{V}_h], \quad (30c)$$

$$\overleftarrow{\mathbf{T}}^{(N+1,N+1)} = 2[(\mathbf{W}^{(N+1)})^{-1}\mathbf{W}_h + (\mathbf{V}^{(N+1)})^{-1}\mathbf{V}_h]^{-1}, \quad (30d)$$

$$\vec{\mathbf{R}}^{(N+1,N+1)} = [(\mathbf{W}_h)^{-1}\mathbf{W}^{(N+1)} + (\mathbf{V}_h)^{-1}\mathbf{V}^{(N+1)}]^{-1} \times [-(\mathbf{W}_h)^{-1}\mathbf{W}^{(N+1)} + (\mathbf{V}_h)^{-1}\mathbf{V}^{(N+1)}]. \quad (30e)$$

Finally, with the above results, we can construct the total $S$-matrix of the whole multilayer $M^{(0,N+1)}$. At the first step, the $S$-matrix $\mathbf{S}^{(0,N)}$ of the multilayer $M^{(0,N)}$ is derived by the Redheffer star product of $\mathbf{S}^{(0,0)}$ of Eq. (29a) and $\mathbf{S}^{(1,N)}$ of Eq. (22a) as

$$\mathbf{S}^{(0,N)} = \mathbf{S}^{(0,0)} * \mathbf{S}^{(1,N)}. \quad (31a)$$

The coupling coefficient matrices $\mathbf{C}_{a,(k)}^{(0,N)}$ and $\mathbf{C}_{b,(k)}^{(0,N)}$ $(1 \leqslant k \leqslant N)$ of the layers $L_1$–$L_N$ in $M^{(0,N)}$ are obtained by, from Eqs. (20c) and (20d):

$$(\mathbf{C}_{a,(k)}^{(0,N)}, \mathbf{C}_{b,(k)}^{(0,N)}) = (\mathbf{C}_{a,(k)}^{(1,N)}(\mathbf{I} - \vec{\mathbf{R}}^{(0,0)}\overleftarrow{\mathbf{R}}^{(1,N)})^{-1}\vec{\mathbf{T}}^{(0,0)}, \mathbf{C}_{b,(k)}^{(1,N)} + \mathbf{C}_{a,(k)}^{(1,N)}(\mathbf{I} - \vec{\mathbf{R}}^{(0,0)}\overleftarrow{\mathbf{R}}^{(1,N)})^{-1}\vec{\mathbf{R}}^{(0,0)}\overleftarrow{\mathbf{T}}^{(1,N)}). \quad (31b)$$

Next, the total $S$-matrix $\mathbf{S}^{(0,N+1)}$ of the multilayer $M^{(0,N+1)}$ is obtained by the Redheffer star product of $\mathbf{S}^{(0,N)}$ of Eq. (31a) and $\mathbf{S}^{(N+1,N+1)}$ of Eq. (30a) as

$$\mathbf{S}^{(0,N+1)} = \mathbf{S}^{(0,N)} * \mathbf{S}^{(N+1,N+1)}. \quad (32a)$$

The final coupling coefficient matrix $\mathbf{C}_{a,(k)}^{(0,N+1)}$ and $\mathbf{C}_{b,(k)}^{(0,N+1)}$ $(1 \leqslant k \leqslant N)$ of the layers $L_1$–$L_N$ in $M^{(0,N+1)}$ is obtained from Eqs. (20a) and (20b):

$$(\mathbf{C}_{a,(k)}^{(0,N+1)}, \mathbf{C}_{b,(k)}^{(0,N+1)}) = (\mathbf{C}_{a,(k)}^{(0,N)} + \mathbf{C}_{b,(k)}^{(0,N)}(\mathbf{I} - \vec{\mathbf{R}}^{(N+1,N+1)}\overleftarrow{\mathbf{R}}^{(0,N)})^{-1}\vec{\mathbf{R}}^{(N+1,N+1)}\vec{\mathbf{T}}^{(0,N)}, \times \mathbf{C}_{b,(k)}^{(0,N)}(\mathbf{I} - \vec{\mathbf{R}}^{(N+1,N+1)}\overleftarrow{\mathbf{R}}^{(0,N)})^{-1}\overleftarrow{\mathbf{T}}^{(N+1,N+1)}). \quad (32b)$$

The $S$-matrix $\mathbf{S}^{(0,N+1)}$ and the coupling coefficient matrices, $\mathbf{C}_{a,(k)}^{(0,N+1)}$ and $\mathbf{C}_{b,(k)}^{(0,N+1)}$, provide the complete characterization of the multilayer $M^{(0,N+1)}$.

## 3. COMPARISON AND DISCUSSION

In this section, the proposed SMM and the conventional SMM are compared. The advantage of the proposed SMM is discussed. First, the conventional field calculation method of the conventional SMM is introduced. In the conventional SMM, only the boundary $S$-matrix that connects the coupling coefficient operators of two layers at both sides of a boundary is used. The boundary condition at the boundary $B_n$ is described by

$$\begin{bmatrix} \mathbf{W}^{(n)}\mathbf{X}^{(n)} & \mathbf{W}^{(n)} \\ \mathbf{V}^{(n)}\mathbf{X}^{(n)} & -\mathbf{V}^{(n)} \end{bmatrix} \begin{bmatrix} \mathbf{C}_{(n)}^{(0,N+1)+} \\ \mathbf{C}_{(n)}^{(0,N+1)-} \end{bmatrix} = \begin{bmatrix} \mathbf{W}^{(n+1)} & \mathbf{W}^{(n+1)}\mathbf{X}^{(n+1)} \\ \mathbf{V}^{(n+1)} & -\mathbf{V}^{(n)}\mathbf{X}^{(n+1)} \end{bmatrix} \begin{bmatrix} \mathbf{C}_{(n+1)}^{(0,N+1)+} \\ \mathbf{C}_{(n+1)}^{(0,N+1)-} \end{bmatrix}. \quad (33)$$

Rearrangement of Eq. (33) gives the conventional boundary $S$-matrix $\hat{\mathbf{S}}^{(n,n)}$:

$$\begin{bmatrix} \mathbf{C}_{(n+1)}^{(0,N+1)+} \\ \mathbf{C}_{(n)}^{(0,N+1)-} \end{bmatrix} = \hat{\mathbf{S}}^{(n,n)} \begin{bmatrix} \mathbf{C}_{(n)}^{(0,N+1)+} \\ \mathbf{C}_{(n+1)}^{(0,N+1)-} \end{bmatrix} = \begin{bmatrix} \vec{\mathbf{t}}^{(n,n)} & \overleftarrow{\mathbf{r}}^{(n,n)} \\ \vec{\mathbf{r}}^{(n,n)} & \overleftarrow{\mathbf{t}}^{(n,n)} \end{bmatrix} \times \begin{bmatrix} \mathbf{C}_{(n)}^{(0,N+1)+} \\ \mathbf{C}_{(n+1)}^{(0,N+1)-} \end{bmatrix}, \quad (34a)$$

where the matrix components of the $S$-matrix are given by

$$\vec{\mathbf{t}}^{(n,n)} = 2[(\mathbf{W}^{(n)})^{-1}\mathbf{W}^{(n+1)} + (\mathbf{V}^{(n)})^{-1}\mathbf{V}^{(n+1)}]^{-1}\mathbf{X}^{(n)}, \quad (34b)$$

$$\overleftarrow{\mathbf{r}}^{(n,n)} = [(\mathbf{W}^{(n+1)})^{-1}\mathbf{W}^{(n)} + (\mathbf{V}^{(n+1)})^{-1}\mathbf{V}^{(n)}]^{-1} \times [-(\mathbf{W}^{(n+1)})^{-1}\mathbf{W}^{(n)} + (\mathbf{V}^{(n+1)})^{-1}\mathbf{V}^{(n)}]\mathbf{X}^{(n)}, \quad (34c)$$

$$\overleftarrow{\mathbf{t}}^{(n,n)} = 2[(\mathbf{W}^{(n+1)})^{-1}\mathbf{W}^{(n)} + (\mathbf{V}^{(n+1)})^{-1}\mathbf{V}^{(n)}]^{-1}\mathbf{X}^{(n+1)}, \quad (34d)$$

$$\vec{\mathbf{r}}^{(n,n)} = [(\mathbf{W}^{(n)})^{-1}\mathbf{W}^{(n+1)} + (\mathbf{V}^{(n)})^{-1}\mathbf{V}^{(n+1)}]^{-1} \times [-(\mathbf{W}^{(n)})^{-1}\mathbf{W}^{(n+1)} + (\mathbf{V}^{(n)})^{-1}\mathbf{V}^{(n+1)}]\mathbf{X}^{(n+1)}. \quad (34e)$$

The total $S$-matrix $\hat{\mathbf{S}}^{(0,N)}$ is given by the consecutive Redheffer star product as the form

$$\hat{\mathbf{S}}^{(0,N)} = \hat{\mathbf{S}}^{(0,0)} * \hat{\mathbf{S}}^{(2,2)} * \cdots * \hat{\mathbf{S}}^{(N,N)} \quad (35a)$$

and holds the relation

$$\begin{bmatrix} \mathbf{C}_{(N+1)}^{(0,N+1)+} \\ \mathbf{C}_{(0)}^{(0,N+1)-} \end{bmatrix} = \hat{\mathbf{S}}^{(0,N)} \begin{bmatrix} \mathbf{C}_{(0)}^{(0,N+1)+} \\ \mathbf{C}_{(N+1)}^{(0,N+1)-} \end{bmatrix} = \begin{bmatrix} \vec{\mathbf{t}}^{(0,N)} & \overleftarrow{\mathbf{r}}^{(0,N)} \\ \vec{\mathbf{r}}^{(0,N)} & \overleftarrow{\mathbf{t}}^{(0,N)} \end{bmatrix} \begin{bmatrix} \mathbf{C}_{(0)}^{(0,N+1)+} \\ \mathbf{C}_{(N+1)}^{(0,N+1)-} \end{bmatrix}. \quad (35b)$$

In the conventional SMM, the internal coupling coefficient operators $\mathbf{C}_{a(b),(n)}^{(0,N+1)+}$ and $\mathbf{C}_{a(b),(n)}^{(0,N+1)-}$ at the $n$th layer $L_n$ are calculated by summing the infinite multiple reflections and transmissions between $M^{(0,n-1)}$ and $M^{(n+1,N+1)}$ as shown in Fig. 5, where the $n$th layer $L_n$ is sandwiched between the left partial multilayer $M^{(0,n-1)}$ and the right partial multilayer $M^{(n+1,N+1)}$.

The partial $S$-matrices $\hat{\mathbf{S}}^{(0,n-1)}$ and $\hat{\mathbf{S}}^{(n,N)}$ are prepared as

$$\hat{\mathbf{S}}^{(0,n-1)} = \begin{bmatrix} \vec{\mathbf{t}}^{(0,n-1)} & \overleftarrow{\mathbf{r}}^{(0,n-1)} \\ \vec{\mathbf{r}}^{(0,n-1)} & \overleftarrow{\mathbf{t}}^{(0,n-1)} \end{bmatrix}, \quad (36a)$$

$$\hat{\mathbf{S}}^{(n,N)} = \begin{bmatrix} \vec{\mathbf{t}}^{(n,N)} & \overleftarrow{\mathbf{r}}^{(n,N)} \\ \vec{\mathbf{r}}^{(n,N)} & \overleftarrow{\mathbf{t}}^{(n,N)} \end{bmatrix}. \quad (36b)$$

The coupling coefficient matrix operators $\mathbf{C}_{a,(n)}^{(0,N+1)+}$, $\mathbf{C}_{a,(n)}^{(0,N+1)-}$, $\mathbf{C}_{b,(n)}^{(0,N+1)+}$, and $\mathbf{C}_{b,(n)}^{(0,N+1)-}$ are, respectively, obtained by the previously used ray-tracing approach as

$$\mathbf{C}_{a,(n)}^{(0,N+1)+} = (\mathbf{I} - \vec{\mathbf{r}}^{(0,n-1)}\overleftarrow{\mathbf{r}}^{(n,N)})^{-1}\vec{\mathbf{t}}^{(0,n-1)}, \quad (37a)$$

$$\mathbf{C}_{a,(n)}^{(0,N+1)-} = \overleftarrow{\mathbf{r}}^{(n,N)}(\mathbf{I} - \vec{\mathbf{r}}^{(0,n-1)}\overleftarrow{\mathbf{r}}^{(n,N)})^{-1}\overleftarrow{\mathbf{t}}^{(0,n-1)}, \quad (37b)$$

$$\mathbf{C}_{b,(n)}^{(0,N+1)+} = \vec{\mathbf{r}}^{(0,n-1)}(\mathbf{I} - \overleftarrow{\mathbf{r}}^{(n,N)}\vec{\mathbf{r}}^{(0,n-1)})^{-1}\vec{\mathbf{t}}^{(n,N)}, \quad (37c)$$

$$\mathbf{C}_{b,(n)}^{(0,N+1)-} = (\mathbf{I} - \overleftarrow{\mathbf{r}}^{(n,N)}\vec{\mathbf{r}}^{(0,n-1)})^{-1}\overleftarrow{\mathbf{t}}^{(n,N)}. \quad (37d)$$

As shown above, in the conventional SMM, constructing two composite $S$-matrices $\hat{\mathbf{S}}^{(0,n-1)}$ and $\hat{\mathbf{S}}^{(n,N)}$ is necessary for finding the coupling coefficients of the $n$th layer $L_n$.

Let us compare the numerical efficiency of the proposed SMM and the conventional SMM in terms of operation counts given in units of floating-point operations per second (flops). Let the operation counts of multiplication, addition (or abstraction), and inversion of $(2H)\times(2H)$ complex matrices be denoted by $m_M$, $m_A$, and $m_I$, respectively. In general, $m_M$ and $m_I$ are proportional to $(2H)^3$ [1,3]. From the definition of the Redheffer star product relation in Eqs. (17a)–(17d), we can count the flops in the star product $\mathbf{S}^{(1,2)} = \mathbf{S}^{(1,1)} * \mathbf{S}^{(2,2)}$ as

$$\mathrm{cnt}(\overleftarrow{\mathbf{R}}^{(1,2)}) = 4m_M + 2m_A + m_I, \quad (38a)$$

$$\mathrm{cnt}(\vec{\mathbf{T}}^{(1,2)}) = 3m_M + m_A + m_I, \quad (38b)$$

$$\mathrm{cnt}(\vec{\mathbf{R}}^{(1,2)}) = 3m_M + m_A, \quad (38c)$$

$$\mathrm{cnt}(\overleftarrow{\mathbf{T}}^{(1,2)}) = 2m_M, \quad (38d)$$

where $\mathrm{cnt}(A)$ means the operation counts in performing the operation $A$ and the common parts shared between Eqs. (17a) and (17d) and Eqs. (17b) and (17c) are taken into consideration. Hence the total operation count of $\mathbf{S}^{(1,2)} = \mathbf{S}^{(1,1)} * \mathbf{S}^{(2,2)}$ is given by the sum of Eqs. (38a)–(38d) as

$$\mathrm{cnt}(\mathbf{S}^{(1,2)}) = 12m_M + 4m_A + 2m_I. \quad (38e)$$

Taking the common parts shared between Eqs. (20a) and (17a), Eqs. (20b) and (17d), Eqs. (20c) and (17b), and Eqs. (20d) and (17c) into account, we can find the operation counts of the star product of coupling coefficient matrices as

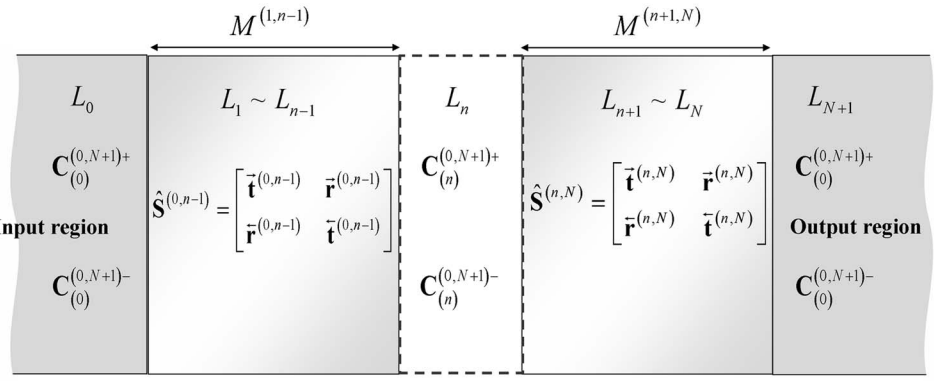


Fig. 5. Coupling coefficient calculation in the conventional SMM.

$$\mathrm{cnt}(\mathbf{C}_{a,(1)}^{(1,2)}) = 2m_M + 2m_A, \tag{39a}$$

$$\mathrm{cnt}(\mathbf{C}_{b,(1)}^{(1,2)}) = 2m_M, \tag{39b}$$

$$\mathrm{cnt}(\mathbf{C}_{a,(2)}^{(1,2)}) = 2m_M, \tag{39c}$$

$$\mathrm{cnt}(\mathbf{C}_{b,(2)}^{(1,2)}) = 2m_M + 2m_A. \tag{39d}$$

Hence the total operation count of $(\tilde{\mathbf{C}}_{a,(1,2)}^{(1,2)}, \tilde{\mathbf{C}}_{b,(1,2)}^{(1,2)}) = (\tilde{\mathbf{C}}_{a,(1,1)}^{(1,1)}, \tilde{\mathbf{C}}_{b,(1,1)}^{(1,1)}) * (\tilde{\mathbf{C}}_{a,(2,2)}^{(2,2)}, \tilde{\mathbf{C}}_{b,(2,2)}^{(2,2)})$ is obtained by the sum of Eqs. (39a)–(39d) as

$$\mathrm{cnt}[(\tilde{\mathbf{C}}_{a,(1,2)}^{(1,2)}, \tilde{\mathbf{C}}_{b,(1,2)}^{(1,2)})] = 8m_M + 4m_A. \tag{39e}$$

Considering the multilayer structure shown in Fig. 1, we can estimate the total operation count, $T_{\mathrm{prop}}$, for performing Eqs. (22a) and (22b) as

$$\begin{aligned} T_{\mathrm{prop}} &= \mathrm{cnt}(\mathbf{S}^{(1,N)}) + \mathrm{cnt}[(\tilde{\mathbf{C}}_{a,(1,N)}^{(1,N)}, \tilde{\mathbf{C}}_{b,(1,N)}^{(1,N)})] = \mathrm{cnt}(\mathbf{S}^{(1,2)} \\ &= \mathbf{S}^{(1,1)} * \mathbf{S}^{(2,2)}) + \mathrm{cnt}(\mathbf{S}^{(1,3)} \\ &= \mathbf{S}^{(1,2)} * \mathbf{S}^{(3,3)}) + \cdots + \mathrm{cnt}(\mathbf{S}^{(1,N)} \\ &= \mathbf{S}^{(1,N-1)} * \mathbf{S}^{(N,N)}) + \mathrm{cnt}[(\tilde{\mathbf{C}}_{a,(1,2)}^{(1,2)}, \tilde{\mathbf{C}}_{b,(1,2)}^{(1,2)})] \\ &\quad + \mathrm{cnt}[(\tilde{\mathbf{C}}_{a,(1,3)}^{(1,3)}, \tilde{\mathbf{C}}_{b,(1,3)}^{(1,3)})] + \cdots + \mathrm{cnt}[(\tilde{\mathbf{C}}_{a,(1,N)}^{(1,N)}, \tilde{\mathbf{C}}_{b,(1,N)}^{(1,N)})] \\ &= (N-1)(12m_M + 4m_A + 2m_I) + [2 + 3 + \cdots + N] \\ &\quad \times (4m_M + 2m_A) = (N-1)(12m_M + 4m_A + 2m_I) \\ &\quad + (N-1)(N+2)(2m_M + m_A) = (2N^2 + 14N - 16)m_M \\ &\quad + (N^2 + 5N - 6)m_A + (2N-2)m_I. \end{aligned} \tag{40}$$

On the other hand, in the case of the conventional SMM, the total operation count of $\hat{\mathbf{S}}^{(1,2)} = \hat{\mathbf{S}}^{(1,1)} * \hat{\mathbf{S}}^{(2,2)}$ is also given by

$$\mathrm{cnt}(\hat{\mathbf{S}}^{(1,2)} = \hat{\mathbf{S}}^{(1,1)} * \hat{\mathbf{S}}^{(2,2)}) = 12m_M + 4m_A + 2m_I. \tag{41}$$

After the partial $S$-matrices $\hat{\mathbf{S}}^{(0,n-1)}$ and $\hat{\mathbf{S}}^{(n,N)}$ are obained for the the $n$th layer $L_n$, the operation counts for obtaining the coupling coefficient matrix operators are given, from Eqs. (37a)–(37d), By

$$\mathrm{cnt}(\mathbf{C}_{a,(n)}^{(0,N+1)+}) = 2m_M + m_A + m_I, \tag{42a}$$

$$\mathrm{cnt}(\mathbf{C}_{a,(n)}^{(0,N+1)-}) = m_M, \tag{42b}$$

$$\mathrm{cnt}(\mathbf{C}_{b,(n)}^{(0,N+1)-}) = 2m_M + m_A + m_I, \tag{42c}$$

$$\mathrm{cnt}(\mathbf{C}_{b,(n)}^{(0,N+1)+}) = m_M. \tag{42d}$$

Thus the total operation count of the conventional SMM, $T_{conv}$, is estimated as

$$\begin{aligned} T_{\mathrm{conv}} &= \mathrm{cnt}((\hat{\mathbf{S}}^{(0,0)}, \hat{\mathbf{S}}^{(1,N)})) + \mathrm{cnt}((\hat{\mathbf{S}}^{(0,1)}, \hat{\mathbf{S}}^{(2,N)})) + \cdots \\ &\quad + \mathrm{cnt}((\hat{\mathbf{S}}^{(0,N-1)}, \hat{\mathbf{S}}^{(N,N)})) \\ &\quad + \mathrm{cnt}[(\mathbf{C}_{a,(1)}^{(0,N+1)+}, \mathbf{C}_{a,(1)}^{(0,N+1)-}, \mathbf{C}_{b,(1)}^{(0,N+1)+}, \mathbf{C}_{b,(1)}^{(0,N+1)-})] + \cdots \\ &\quad + \mathrm{cnt}[(\mathbf{C}_{a,(N)}^{(0,N+1)+}, \mathbf{C}_{a,(N)}^{(0,N+1)-}, \mathbf{C}_{b,(N)}^{(0,N+1)+}, \mathbf{C}_{b,(N)}^{(0,N+1)-})] \\ &= N[(N-1)(12m_M + 4m_A + 2m_I) + 6m_M + 2m_A + 2m_I] \\ &= (12N^2 - 6N)m_M + (4N^2 - 2N)m_A + 2N^2 m_I. \end{aligned} \tag{43}$$

Let us estimate the difference between the operation counts of the conventional SMM, $T_{\mathrm{conv}}$, and those of the proposed SMM, $T_{prop}$:

$$\begin{aligned} T_{\mathrm{conv}} - T_{\mathrm{prop}} &= (10N^2 - 20N + 16)m_M + (3N^2 - 7N + 6)m_A \\ &\quad + (2N^2 - 2N + 2)m_I \gg 0. \end{aligned} \tag{44}$$

Therefore we can see that, in terms of the operation counts, the proposed SMM is superior to the conventional SMM. The reason is that in the proposed SMM, the $S$-matrix and the coupling coefficient matrices evolve together at each stage, whereas in the conventional SMM, the coupling coefficient matrices are found in just the independent postprocess, including the calculation of $\hat{\mathbf{S}}^{(0,n-1)}$ and $\hat{\mathbf{S}}^{(n,N)}$, which generally requires a heavy computational cost as estimated in Eq. (43). This difference between the proposed SMM and the conventional SMM with respect to the computational efficiency becomes more noticeable as the number of layers and the size of matrices increase. This is actually a main computational limitation of the conventional SMM [4]. However, the proposed SMM with the newly defined Redheffer star product of the coupling coefficient operators may overcome the computational inefficiency of the conventional SMM.

In Section 1, two types of parallelism were addressed. The first is the transversal parallelism using the matrix parallel computation with parallel linear algebra libraries such as the SCALAPACK. In this parallelism, the computation overhead is relatively high since each matrix operation is performed with accompanying continuous message-passing interface communication. However, the second parallelism that was mainly focused on is the longitudinal parallelism based on the inherent structure of the SMM. In this parallelism, the communication between CPUs does not often occur. The strategy of the longitudinal parallelism is just divide and solve. In other words, before using the binary scheme, all CPUs can work independently without any necessary communication with other CPUs. Until this stage, the numerical efficiency of the parallelism using $M$ CPUs is exactly $M$ times over the serial computation, since there is not significant communication overhead. After finishing its own computation of the partial $S$-matrices and partial coupling coefficient matrices, a CPU in a pair of two CPUs passes its calculation results, that is, $S$-matrix and coupling coefficient matrices of its partial multilayer, to its neighbor CPU. And then the receiving CPU works to combine two adjacent partial multilayers. In this work, the communication between two CPUs is very simple and just once occurs. This type of simple communication, just data transfer, can be realized by data transfer through direct networking or writing and reading on common hard

disks. Usually, the operation time required for this simple data transfer is relatively very small compared with the main matrix computation of RCWA and the $S$-matrix operation. Actually, in the first transversal parallelism, the computational overhead accompanying the use of the SCALAPACK would be important. However, in this paper, just the second parallelism is focused on and discussed. Therefore, in the proposed SMM, just data transfer would be the elements of possible overhead. Thus, it can be said that the computational overhead inherent in the second parallelism (longitudinal parallelism) is small, and so the enhancement factor of using $M$ CPUs would be approximately $M$ times over using just serial computation with a single CPU.

On the other hand, the most notable functional advantage of the proposed SMM is the functional block-based FMM as illustrated in Fig. 6. The most important application of the associative rule of the SMM is the functional block-based FMM, where with the $S$-matrix information from independently analyzed two-block systems, A and B, we can completely characterize the combined system of two blocks. In the conventional SMM, the characterization of the input and output properties of the total $S$-matrix is generally considered. However, when obtaining the internal field distributions, the conventional SMM recalculates all internal coupling coefficients of the combined system using the above-described method. This classical algorithm is very inefficient and a main origin of the computational limitation of the conventional SMM. Our refined Redheffer star product relation of the coupling coefficient matrices of the proposed SMM actually overcomes this limitation. We can obtain the internal field distribution very efficiently by the simple step described in Eq. (21). Therefore the proposed SMM is a very effective tool for the functional block-based FMM.

In addition, our refined Redheffer star product relation of the coupling coefficients enables the efficient parallel binary-tree computation of the extended SMM. We can effectively exploit the parallelism of the proposed SMM by adopting the parallel binary-tree scheme in the practical computation. Let us assume that the total number of the bodies of the multilayer $N$ is $N=K\times M$, where $K$ is a positive integer and $M$ is the number of nodes of the parallel computer used for the computation. In addition, the node number $M$ is assumed to be $M=2^p$. In this configuration, we can divide the multilayer structure into $M$ blocks composed of $K$ layers as shown in Fig. 7. Since the parallel computer has $M$ CPUs, the $m$th CPU in the parallel computer should calculate the $S$-matrix of the $m$th block in a serial manner. After achieving the characterization information of all blocks using the extended SMM, we can combine the $S$-matrices and the coupling coefficient matrix operators of all blocks by using the binary-tree approach. For a systematic description, let the index sets be defined as

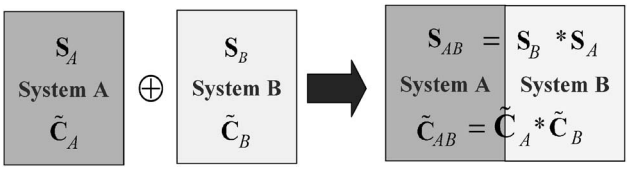


Fig. 6. Functional block-based FMM.

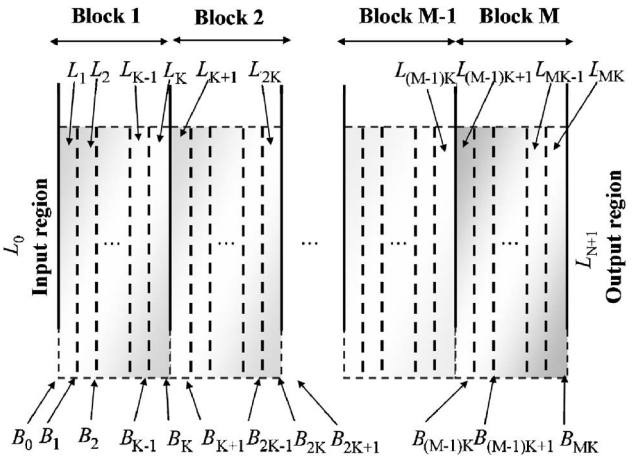


Fig. 7. Multilayer structure divided into $M$ blocks containing $K$ layers.

$$M_p = \{m_{(p)} | m_{(p)} = 1,2,3,\ldots,2^p\} \quad \text{for } p = 0,1,\ldots,\log_2 M, \tag{45}$$

and let the $S$-matrix and the coupling coefficient matrices of $m_{(p)}$ be denoted by $\tilde{\mathbf{S}}_{(p)}^{(m_{(p)})}$, $\tilde{\mathbf{C}}_{a,(p)}^{(m_{(p)})}$, and $\tilde{\mathbf{C}}_{b,(p)}^{(m_{(p)})}$. At the first stage, the $(2m_{(p)-1})$th block and the $(2m_{(p)})$th block are combined in to a single block. After the combination, the index set is changed to $M_{p-1}$. The constructed block is denoted by the $(m_{(p-1)})$th block in the index set $M_{p-1}$. The total number of blocks is $2^{P-1}$. This process is denoted by

$$\tilde{\mathbf{S}}_{(p-1)}^{(m_{(p-1)})} = \tilde{\mathbf{S}}_{(p)}^{(2m_{(p)}-1)} * \tilde{\mathbf{S}}_{(p)}^{(2m_{(p)})}, \tag{46a}$$

$$(\tilde{\mathbf{C}}_{a,(p-1)}^{(m_{(p-1)})}, \tilde{\mathbf{C}}_{b,(p-1)}^{(m_{(p-1)})}) = (\tilde{\mathbf{C}}_{a,(p)}^{(2m_{(p-1)}-1)}, \tilde{\mathbf{C}}_{b,(p)}^{(2m_{(p-1)}-1)}) * (\tilde{\mathbf{C}}_{a,(p)}^{(2m_{(p-1)})}, \tilde{\mathbf{C}}_{b,(p)}^{(2m_{(p-1)})}). \tag{46b}$$

By $p$ iterations of the recursion equations, we finally obtain the total $S$-matrix of the multilayer body $\mathbf{S}^{(1,N)} \times (=\tilde{\mathbf{S}}_{(0)}^{(1)})$. It is noted that this parallel binary scheme for obtaining the coupling coefficient matrices cannot be constructed within the conventional SMM, since in the conventional SMM the computation of the coupling coefficients is an independent postprocessing after finding the total $S$-matrix, and so its algorithm structure cannot be distributable on the binary-tree structure. However, in the proposed SMM, through the Redheffer star product relation of the coupling coefficient matrices, the parallel binary-tree computation is naturally adopted for obtaining the coupling coefficient matrices. Regarding the memory requirement on the parallel computing environment, the construction of the necessary partial $S$-matrices in the conventional SMM does not have advantages over the proposed SMM, since each partial layer requires its own memory containing all primitive $S$-matrices of single layers for calculating its own specifically formed $S$-matrix pair.

## 4. NUMERICAL RESULTS

In this section, the RCWA examples of the proposed SMM and the ETMM are compared to prove the validity of the

proposed SMM. We examine the RCWA results of the three-dimensional circular dielectric fiber-tip structure shown in Fig. 8(a). The original continuous structure is approximately modeled by the staircase multilayer structure of 16 layers as shown in Fig. 8(b). The first layer is the half-infinite circular fiber structure, and the last layer is the half-infinite free space. Thus the body of the tip is composed of 14 layers. In this example, the wavelength of

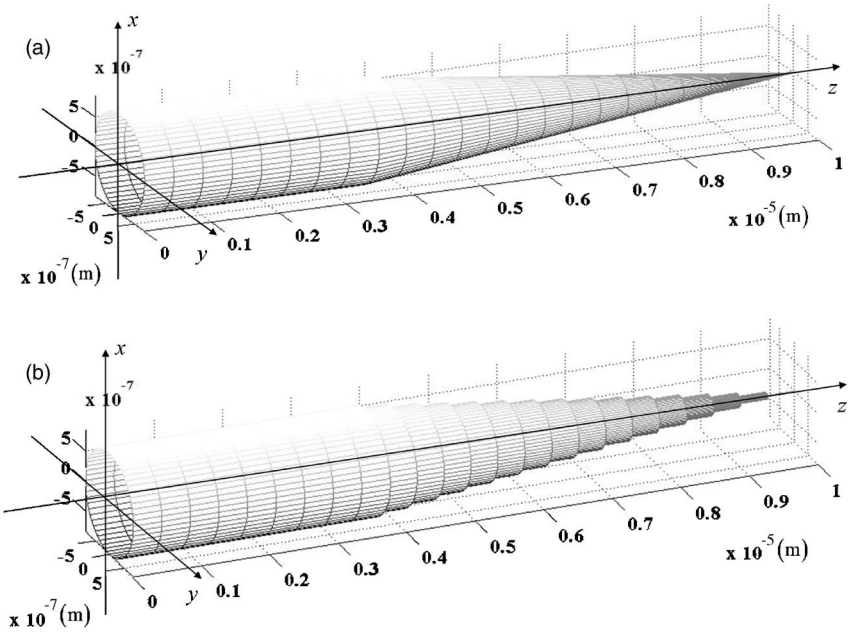


Fig. 8. Example target structure: (a) dielectric fiber tip, (b) multilayer structure modeling of the fiber tip with the staircase approximation.

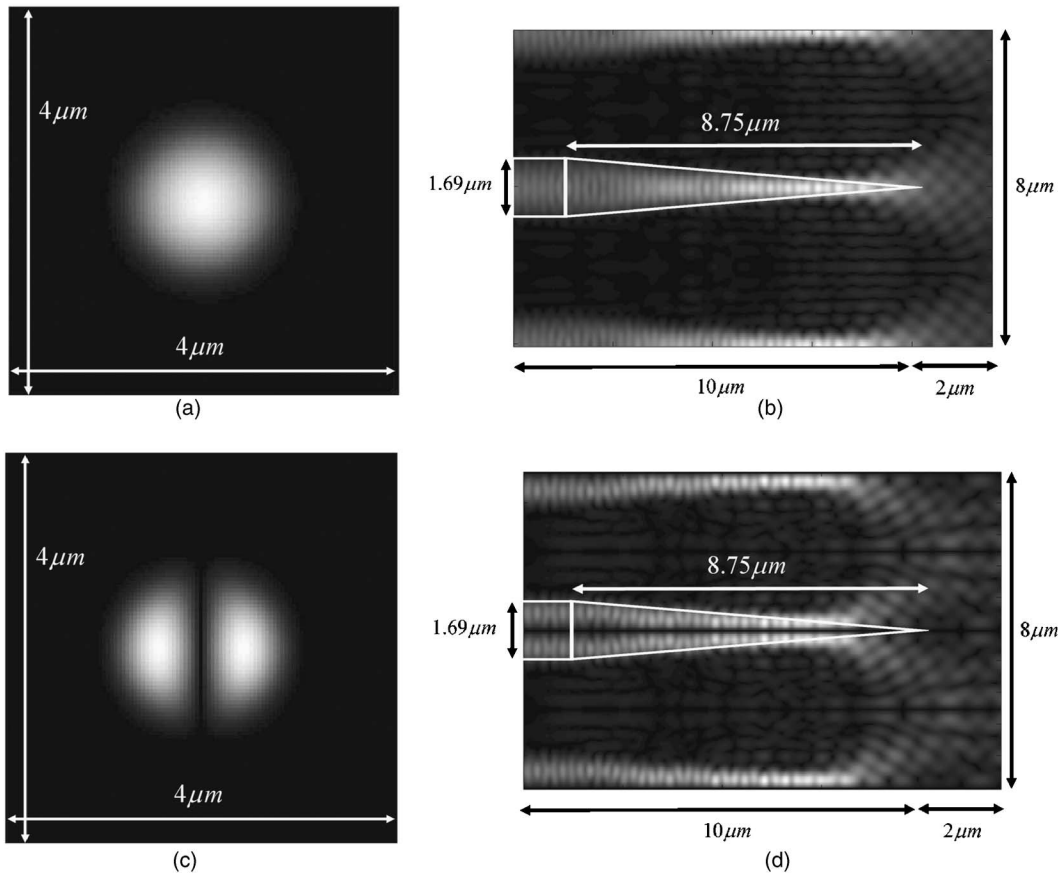


Fig. 9. (a) First selected input mode profile (in the $x-y$ plane), (b) excited electric field distribution (in the $z-x$ plane), (c) second selected input mode profile (in the $x-y$ plane), (d) excited electric field distribution (in the $z-x$ plane).

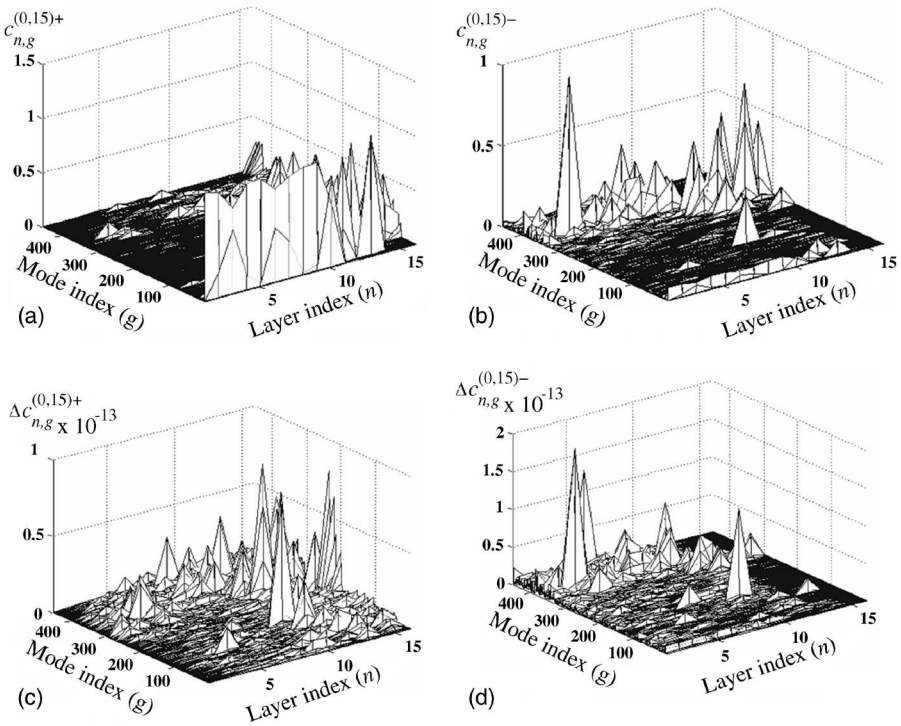


Fig. 10. (a) Coupling coefficients of the positive eigenmodes and (b) those of the negative eigenmodes excited by the first selected input mode; (c) the deviation between the coupling coefficients of the positive modes obtained by the proposed SMM and by the ETMM; (d) the deviation between the coupling coefficients of the negative modes obtained by the proposed SMM and by the ETMM.

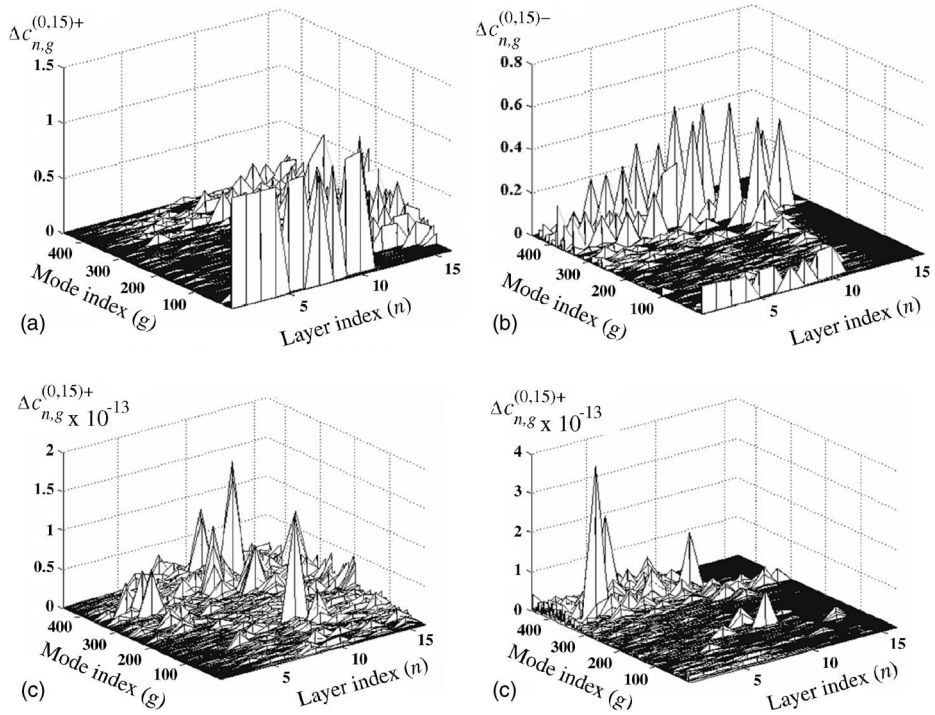


Fig. 11. (a) Coupling coefficients of the positive eigenmodes and (b) those of the negative eigenmodes excited by the second selected input mode; (c) the deviation between the coupling coefficients of the positive modes obtained by the proposed SMM and by the ETMM; (d) the deviation between the coupling coefficients of the negative modes obtained by the proposed SMM and by the ETMM.

the optical field is 632.8 nm, both the $x$-direction and the $y$-direction periods are 4 $\mu$m, the fiber diameter in the input region is 1.69 $\mu$m, the tip length is 8.75 $\mu$m, and the refractive index of the fiber tip is 1.5. The numbers of the $x$-direction and $y$-direction transverse Fourier frequencies used in the RCWA are equally set to 15.

Since the input region is a circular fiber structure, we can selectively choose the incidence mode profiles among

several eigenmodes of the fiber structure. Figures 9(a) and 9(c) show the transverse electric field profiles of the first and second selected modes. The electric field distributions in the vertical cross-section plane (in the $x-z$ plane) for the incidence of the first and second modes obtained by using the proposed SMM are visualized in Figs. 9(b) and 9(d), respectively. We can observe clear differences in the diffraction patterns of the electric fields of the two incidence modes.

In addition, the obtained results of the proposed SMM are compared with those of the ETMM. The distributions of the coupling coefficients $c_{n,g}^{(0,15)+}$ and $c_{n,g}^{(0,15)-}$ for the first incidence mode obtained by the proposed SMM are plotted in Figs. 10(a) and 10(b), respectively. These distributions are obtained from Eqs. (11e) and (11f). The coupling coefficient distributions are also calculated with the ETMM for comparison. Then the deviations $\Delta c_{n,g}^{(0,15)+}$ and $\Delta c_{n,g}^{(0,15)-}$ between the coupling coefficient distributions obtained by the SMM and those by the ETMM are presented in Figs. 10(c) and 10(d), respectively. As a result, we can see that the deviations are negligible and the result of the SMM agrees highly with that of the ETMM. In Figs. 11(a) and 11(b), the coupling coefficient distributions obtained for the second incidence mode through the same manner are plotted. The deviations between the results of the SMM and those of the ETMM are presented in Figs. 11(c) and 11(d). Also, in this case, the deviations are negligible, and the result of the SMM agrees highly with that of the ETMM. Furthermore, we can confirm that the coupling coefficient matrix obtained by the SMM does totally agree with that obtained by the ETMM. By these comparisons, the validity of the proposed scheme is proved.

## 5. CONCLUSION

In this paper, an extended and refined SMM is proposed for the efficient full parallel implementation of the FMM. The motivation of this study is to overcome the computational limitation of the conventional SMM. The main result is the Redheffer star product relation of the coupling coefficient operators and the following refinement of the SMM. In this paper, it is shown that the proposed SMM is successfully applied to the RCWA. However, the proposed scheme is so general that it can also be adopted in other FMMs using a multilayer-based structure modeling such as the pseudo-Fourier modal analysis method. The complete parallel implementation of the FMMs through the proposed SMM is a requisite for the functional block-based Fourier modal analysis of various photonic circuit structures requiring large-scale parallel computation.

## REFERENCES


1. L. Li, "Formulation and comparison of two recursive matrix algorithms for modeling layered diffraction gratings," J. Opt. Soc. Am. A **13**, 1024–1035 (1996).
2. E. L. Tan, "Note on formulation of the enhanced scattering-(transmittance-) matrix approach," J. Opt. Soc. Am. A **19**, 1157–1161 (2002).
3. L. Li, "Note on the *S*-matrix propagation algorithm," J. Opt. Soc. Am. A **20**, 655–660 (2003).
4. M. G. Moharam and A. B. Greenwell, "Efficient rigorous calculations of power flow in grating coupled surface-emitting devices," Proc. SPIE **5456**, 57–67 (2004).
5. M. G. Moharam, E. B. Grann, and D. A. Pommet, "Formulation for stable and efficient implementation of the rigorous coupled-wave analysis of binary gratings," J. Opt. Soc. Am. A **12**, 1068–1076 (1995).
6. P. Lalanne and G. M. Morris, "Highly improved convergence of the coupled-wave method for TM polarization," J. Opt. Soc. Am. A **13**, 779–784 (1996).
7. P. Lalanne, "Improved formulation of the coupled-wave method for two-dimensional gratings," J. Opt. Soc. Am. A **14**, 1592–1598 (1997).
8. E. Silberstein, P. Lalanne, J. P. Hugonin, and Q. Cao, "Use of grating theories in integrated optics," J. Opt. Soc. Am. A **18**, 2865–2875 (2001).
9. P. Lalanne and E. Silberstein, "Fourier-modal methods applied to waveguide computational problems," Opt. Lett. **25**, 1092–1094 (2000).
10. H. Kim, S. Kim, I.-M. Lee, and B. Lee, "Pseudo-Fourier modal analysis on dielectric slabs with arbitrary longitudinal permittivity and permeability profiles," J. Opt. Soc. Am. A **23**, 2177–2191 (2006).
11. H. Kim and B. Lee, "Analysis of TIR holography using pseudo-Fourier modal analysis method," Proc. SPIE **6314**, 63141C (2006).
12. M. G. Moharam, D. A. Pommet, and E. B. Grann, "Stable implementation of the rigorous coupled-wave analysis for surface-relief gratings: enhanced transmittance matrix approach," J. Opt. Soc. Am. A **12**, pp. 1077–1086 (1995).